VTA dopamine neurons drive spatiotemporally heterogeneous striatal dopamine signals during learning

Liv Engel[1,2,3,#], Amy R Wolff PhD[1,2,#], Madelyn Blake[1,2], Val L. Collins PhD[1,2], Sonal Sinha[4], Benjamin T Saunders PhD[1,2]

[1] *Department of Neuroscience, University of Minnesota*
[2] *Medical Discovery Team on Addiction, University of Minnesota*
[3] *Current Address: Department of Psychology, University of Toronto*
[4] *Johns Hopkins University*
[#] *Denotes equal contribution*

Correspondence: BTS (bts@umn.edu, @bensaunders, saunderslab.com)

PREPRINT

Environmental cues, through Pavlovian learning, become conditioned stimuli that guide animals toward the acquisition of rewards (for example, food) by invigorating and directing seeking behavior. Dopamine neurons are crucial for this process, by signaling information related to rewards, as well as associated actions, states, and cues. Dopamine neurons are embedded in a reciprocally connected network with their targets in the striatum, the functional relevance of which remains poorly understood. Here we investigated how cue-evoked behavior generated by dopamine neurons is signaled by dopamine release downstream in striatal subregions and how they evolve across stages of learning. We made use of a genetically encoded dopamine biosensor (dLight) to monitor dopamine signaling in the nucleus accumbens (NAc) core and shell, dorsomedial striatum (DMS), and dorsolateral striatum (DLS) with fiber photometry, while tracking detailed movement features during optogenetic Pavlovian cue conditioning of VTA dopamine neurons. We demonstrate spatially heterogeneous, learning-dependent changes across striatal regions. Cues paired with optogenetic activation of VTA dopamine neurons evoked dopamine release preferentially in the NAc core, but not shell, early in training, when behavioral responses were slower and directed toward the cue. Critically, these NAc core signals remained stable, and as training progressed, VTA cue-evoked dopamine signals also emerged in the DMS. Further, prediction error signals, reflecting a violation in the expectation of dopamine neuron activation, only emerged in the NAc core and DMS. Despite the development of rapid, vigorous movement late in training, conditioned dopamine signals did not emerge in the DLS. Together our studies show broad dissociation in the fundamental prediction and reward-related information signaled by dopamine across the striatum. Further, they offer new insight into how larger-scale plasticity across the striatal dopamine network emerges during Pavlovian learning to coordinate behavior.

INTRODUCTION

Behavior is heavily influenced by external sensory information ("cues") that acquires motivational value to trigger and guide complex behaviors. Midbrain dopamine neuron activity, and dopamine signals in the striatum, is crucial for learning and evaluation of cues, actions, and biologically relevant outcomes during decision making (1–5). Dopamine neuron activity is evoked by rewards and can substitute for rewards to drive cue-based learning and motivation, with heterogeneous functions ascribed to different subcircuits (6–13).

Dopamine neurons project largely along an ipsilateral, ventromedial to dorsolateral gradient, with ventral tegmental area (VTA) neurons preferentially innervating the ventral and medial striatum, and substantia nigra (SNC) neurons preferentially innervating the dorsal and lateral striatum (14–16). Through direct and indirect circuits back from the striatum to the midbrain, this network is thought to be functionally organized as an ascending "spiral" (16,17), where the locus of control of learning and behavioral execution transitions from dopamine inputs into the nucleus accumbens (NAc) to dopamine inputs into the dorsolateral striatum (DLS) (18–20). This transition is thought to parallel the emergence of stereotyped, habitual action patterns seen with extended training (21–23). Recent work has complicated this influential framework, however, with studies showing a lack of DLS recruitment (24,25), no reduction in NAc dopamine signaling (26,27), and a maintenance of NAc control of behavior late in conditioning (28). In parallel, there is growing consensus of highly specialized dopamine signaling patterns and functional roles among dopamine projections and the striatal niches they innervate (6,8,29–35).

Despite the implications for a more complete understanding of the functional architecture of the striatal network, it remains unknown how dopamine neuron activity engages dopamine signals broadly throughout the striatum, across different phases of learning. To establish the impact of VTA dopamine neuron activity during Pavlovian learning on cue and movement relat-

ed dopamine signaling across four major striatal subregions: the nucleus accumbens (NAc) medial shell, NAc core, dorsomedial striatum (DMS), and the dorsolateral striatum (DLS) we combined optogenetic manipulation of dopamine neurons with simultaneous recording of striatal dopamine transmission using the biosensor dLight (36) and pose estimation (37) for detailed behavioral analysis. Brief dopamine neuron activation drove learning about antecedent cues, and these cues came to evoke conditioned approach and rapid movement invigoration across training, similar to learning driven by external rewards (6,38,39). Dopamine signal dynamics during this dopamine-driven Pavlovian learning were spatiotemporally heterogeneous. Cue-evoked dopamine signals emerged early in training in the NAc core, but not shell, and then later emerged in the DMS. NAc core and DMS dopamine signals were also selectively sensitive to prediction errors related to dopamine neuron activity. Despite extended training that promoted vigorous cue-evoked movement, NAc core signals did not diminish and cue-evoked signals in the DLS did not emerge.

Our results indicate that extended Pavlovian learning mediated by dopamine neuron activity leads to a preferential recruitment of cue, reward, and error-related dopamine signals in only a subset of striatal targets. Further, our data suggest that extended Pavlovian learning does not produce a ventral to dorsal striatal shift in dopamine signaling. Instead, dopamine neurons engage broad recruitment of striatal dopamine signaling during learning across different timescales, with unique subregion-based profiles.

RESULTS

VTA dopamine neurons drive cue learning and vigorous behavior

For manipulation of dopamine neurons, we expressed the red-shifted excitatory opsin Chrimson in TH-cre rats (6,40), which resulted in selective targeting in the VTA (**Figure 1A**). To investigate the ability of sensory cues paired with activation of VTA dopamine neurons to drive behavioral invigoration, we made use of an optogenetic Pavlovian conditioning procedure 6. Rats first underwent habituation to a novel, neutral cue (light+tone, 7 sec), followed by 20 daily sessions where the cue was paired with laser delivery to the VTA (589 nm, 20Hz, 2mW pulses, 5 sec) 25 times per session (**Figure 1B; Supplemental Figure 1**). Laser stimulation began 2 sec after cue onset. No other reward or external stimuli were administered.

We first analyzed a subset of video recordings of training sessions (n=10 rats) via experimenter inspection. Rats quickly exhibited conditioned behavioral responses (CRs), first defined simply as locomotion, which increased in probability across training during cue presentations (**Figure 1C**; probability of locomotion in first 2-sec of cue, mixed-effects ANOVA main effect of session, $F(1.53,13.04)=15.75$, $p=.0006$). Conditioned movement emerged at shorter onset latency as training progressed, with the large majority of CRs beginning during the first 2-sec of the cue, before laser onset (**Figure 1D**; $F(1.84,11.93)=12.62$, $p=.0013$). This replicates previous findings (6), indicating that CRs elicited by dopamine-paired cues were learned behavioral responses, and not simply triggered by laser activation of dopamine neurons. We have also previously demonstrated (6) that this conditioned invigoration is dependent on temporal contiguity between the cue and dopamine neuron activation: unpaired, uncued optogenetic activation of dopamine neurons in either the VTA or SNC is insufficient to drive cue learning, and does not evoke movement or other behaviors (27,43). For more detailed quantification of cue-evoked behavior across the whole dataset (n=20 rats), we employed DeepLabCut (37) for movement analysis (**Supplemental Figure 2**). This revealed that the latency of movement onset after cue onset decreased (mixed effects ANOVA main effect of training phase, $F(1.7,28.8)=3.79$, $p=.041$) and the duration of movement bouts during cue presentations increased ($F(1.51,25.59)=22.04$, $p<.0001$) across early (days 1-2), middle (days 11-12), and late (days 19-20) training phases. The average (**Figure 1E,F**) and maximum speed (**Figure 1G**) of conditioned movement both increased across training ($F(1.81,30.81)=25.65$, $p<.0001$; $F(1.928,32.78)=21.52$, $p<.0001$). Further, the vigor of conditioned movement accelerated across training, reflected in a decreased latency to achieve maximum speed (**Figure 1H**; $F(1.44,24.43)=327.9$, $p<.0001$). While maximum speed leveled off between the middle and late training phases (**Figure 1G**), movement acceleration continued to increase into the late phase (**Figure 1I**). These changes in movement speed reflected a conditioned, cue-dependent invigoration state, as examination of speed during the 5 seconds before cue onset show no changes across training (Average pre cue speed, no effect of training phase, $F(1.99,33.9)=.036$, $p=.964$); Max pre cue speed, no effect of training phase, $F(1.92, 32.6)=1.44$, $p=.858$).

We analyzed behavioral data split by both phase and sex (12 F, 8 M). Overall, female rats had a higher average cue-evoked movement speed than males at each training phase (**Supplementary Figure 3B**; 2-way

mixed effects ANOVA main effect of sex, F(1,18)=4.42, p=.0499). This reflected a general sex difference in movement, rather than a sex-specific difference in dopamine-mediated learning, as females also had a higher pre-cue movement speed across all training phases (2-way mixed effects ANOVA main effect of sex, F(1,18)=4.65, p=.045). We found no other sex-based differences in behavioral measures (**Supplementary Figure 3**; all sex comparisons p>.05).

The visual component of the cue complex was a circular illuminated panel positioned at rearing height on one wall of the chamber. This allowed, as with our previous studies (6), for localized, cue-directed CRs to occur, in the form of orientation, approach, and investigation (**Figure 2**), a common behavioral response to reward-predictive cues (44). We quantified cue approach behavior in two ways. First, experimenters recorded instances of approach. Approach behavior was evident early in training, on approximately one-third of cue presentations, and stayed relatively consistent throughout conditioning (**Figure 2B**, approach number: mixed effects ANOVA trend for training phase, F(2.79,23.73)=2.98, p=0.0525; **Figure 2C**, approach probability: F(2.65,22.55)=2.87, p=0.064).

For further behavioral characterization, we next used a semi-automated behavioral classification method, based on rat position and body posture data from the DeepLabCut model. Behavioral classification based on DLC position data was highly consistent with human-based video scoring but allowed for a more detailed assessment of cue-directed behavior. Automated detection of approach using the DLC-based positional location of the nose relative to the cue was classified as periods when the animals nose approached the cue for periods longer than 0.2s in duration. In line with our manually scored data, this analysis showed that approach behavior developed early in Pavlovian training and was broadly consistent throughout. There was a decreasing trend in the likelihood of approaches initiated after cue onset from early to late training days (**Figure 2D**, Percentage cue periods with an approach: mixed effects ANOVA main effect of training phase, F(1.716,29.17)=3.43, p=0.052). Approach latency was stable across training (**Figure 2E**, latency: F(1.67,26.78)=0.25, p=.74). Animals did, however, spend less time overall engaged in cue approach from early to later phases of training (**Figure 2F**, approach duration: F(1.44,24.41)=11.07, p=.001) and the time spent interacting with the cue on approach trials decreased from early to later training phases (**Figure 2G**, F(1.85,29.51)=5.00, p=.01).

We also assessed orientation to the cue, as a measure of cue-directed attention that did not meet the threshold of approach. We calculated head direction, based on interpolation of a vector projecting from the cranial implant to the nose, which allowed for quantification of head angle compared to other features of

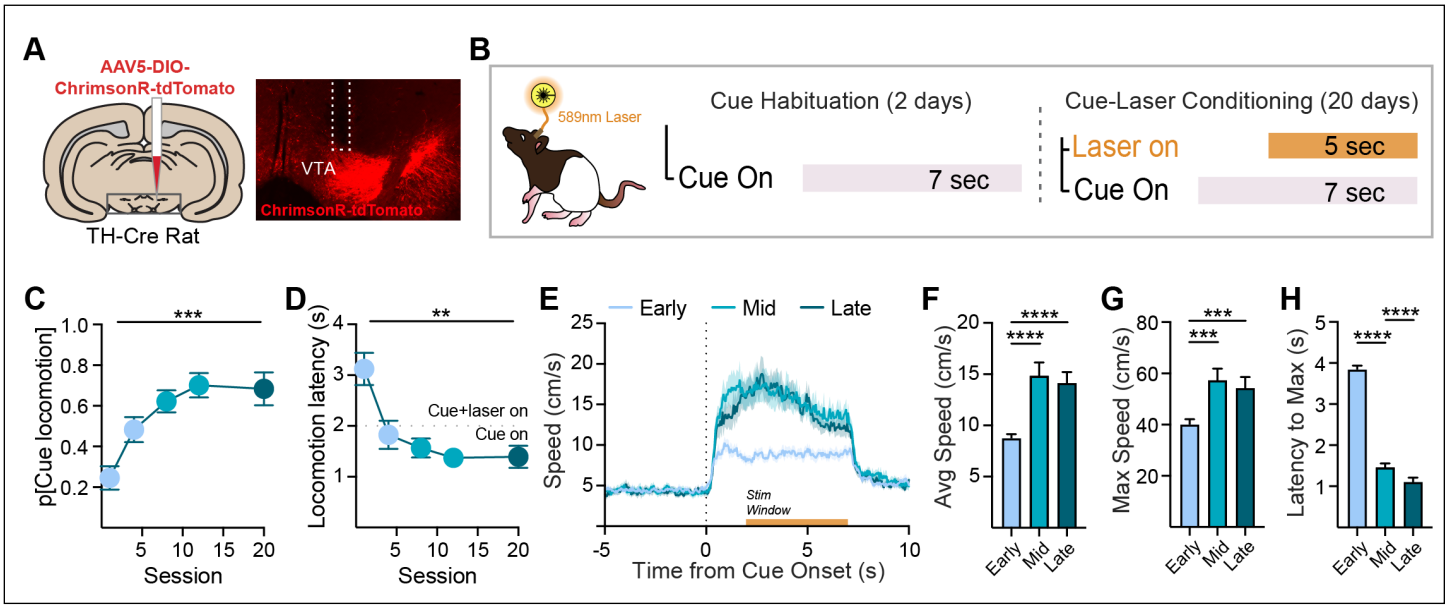

Figure 1. VTA dopamine neurons drive cue learning and vigorous behavior. A) ChrimsonR-tdTomato was selectively expressed in dopamine neurons in TH-cre rats (N=20) and optic fibers were inserted over viral expression in the VTA. B) Schematic of optogenetic Pavlovian conditioning procedure. Following habituation to a novel, neutral cue (light + tone), rats underwent training where the cue was paired with laser (589 nm) delivery 20 times per session for 20 sessions. C) Across this training, conditioned responses (movement) emerged with high probability in the first 2-sec of the cue period. D) The latency of locomotion onset decreased across sessions and the majority of responses were initiated less than 2-sec after cue onset, indicating they were cue, rather than laser evoked. E) Movement was tightly locked to cue onset, increasing in speed across the early (days 1-2), middle (days 11-12), and late (days 19-20) phases of training. Both average F) and maximum G) speed achieved increased between early and middle/late training phases. H) Movement acceleration, reflected in the decreased time required to reach maximum speed, increased between each training phase. ****p<.0001, ***p<.001, **p<.01.

the environment (**Supplemental Figure 2**). Given that the cue light was in a fixed position relative to the rat, orientation behavior was interpreted as a reduction in head-to-cue angle (< 30°, 0.2s duration). The likelihood of orientation to the cue increased from early to later stages of training (**Figure 2H**, Percentage of trials: mixed effects ANOVA main effect of training phase, F(1.476,25.08)=9.05 p<.0.01), with a consistent onset latency (**Figure 2I**, F(1.71,29.14)=1.36, p=.27). However, on trials where animals did orient to the cue, the total time orienting (**Figure 2J**, F(1.98,33.64)=8.88, p=.0008) and the duration of the initial orientation (**Figure 2K**, F(1.56,26.45)=5.53, p=.01) decreased significantly in the later stages of training. Thus, overall, rats maintained attention to the cue across training, but spent less time engaged in cue investigation.

As training progressed, we observed an evolution in

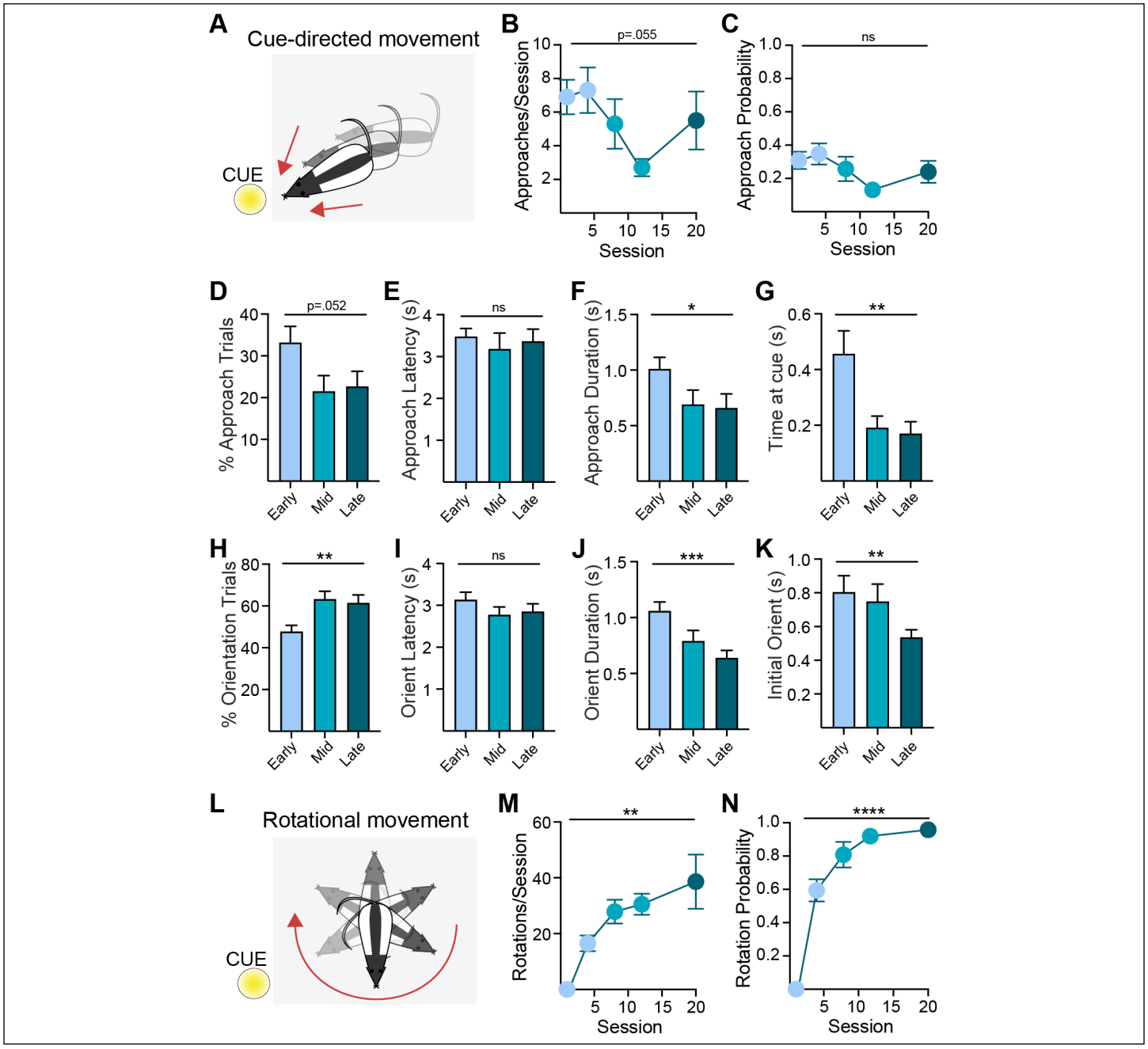

Figure 2. Behavior transitions from cue-directed to general invigoration with extended dopamine-mediated learning. A) Rats (n=20) developed conditioned behavioral responses directed at the cue. Approach behavior was manually scored by experimenters. These responses emerged early in training but remained consistent in B) number and C) probability at later stages. D) Further classification using semi-automated pose estimation data showed a trend towards a decrease in the percentage of trials containing an approach response across training. E) The latency to approach was stable across training phases. F) Initial approach duration and G) the time rats spent at the cue decreased across training phases. H) The percent of trials on which rats oriented to the cue, measured by comparing the rat's head direction to the cue position, increased across training while I) the latency of cue orientation was stable. J) The total time spent orienting and the K) length of the initial orientation decreased across training. L) As training progressed, cue-evoked movement evolved into a more vigorous, rotational pattern, as rats ran in circles around the chamber. Rotation did not occur early in training but increased robustly in M) number and N) probability across training. ****p<.0001, ***p<.001, **p<.01, *p<.05.

conditioned behavior, where rats transitioned from predominantly linear movement often directed at the cue, to more vigorous rotational behavior around the perimeter of the chamber (**Figure 2L, Supplementary Figure 2**). This turning behavior was cue-evoked, and always occurred contralateral to the stimulation site. Rotational behavior was quantified via video inspection. Rotations never occurred in the first few sessions of training, indicating they reflect a learned CR rather than a simple laser-evoked movement pattern. Across the middle and later training stages, rotational movement strongly emerged, increasing in number (**Figure 2M**, Mixed effects ANOVA main effect of training phase, $F(1.44,12.25)=12.83$, $p=.0019$) and probability (**Figure 2N**, $F(1.98,16.84)=77.39$, $p<.0001$) during cue presentations.

Together these results show that, via association with VTA dopamine neuron activation, cues acquired Pavlovian conditioned stimulus properties, driving robust CRs that became more vigorous and less cue directed with extended dopamine-mediated learning.

VTA dopamine mediated learning drives cue-evoked dopamine signals first in the core, then DMS, but not in shell or DLS

Cues paired with natural rewards evoke dopamine neuron activity and release at dopamine neuron targets (12,13,31,45). We previously showed that dopamine neurons also develop conditioned activity in response to cues predictive of their optogenetic activation (6). Here, we assessed the extent to which VTA dopamine-paired cues evoke dopamine signaling downstream in the striatum (**Figure 3A**), using fiber photometry recordings of the dLight1.3b sensor (36). Dopamine signaling was measured across four striatal regions: the NAc medial shell, NAc core, DMS, and DLS (**Supplemental Figures 5**). Across all sites, we found robust spontaneous dopamine signals (**Figure 3B,C**).

We recorded dLight signals at these sites across optogenetic Pavlovian conditioning of VTA dopamine neurons (**Figure 4A**). Spatially and temporally heterogeneous dopamine signals emerged in response to VTA dopamine neuron predictive cues (**Figure 4B-E**). Cue-evoked increases in dopamine developed in the NAc core and the DMS, but not in the medial shell or DLS. NAc core signals emerged first, early in training, and remained stable (**Figure 4C**). In contrast, DMS signals were not present early in training, but emerged by the middle phase (**Figure 4D**) once behavior had largely stabilized. For the core and DMS, dopamine signals peaked around 800 ms after cue onset, before laser stimulation began. Despite the development of rapid and vigorously expressed movement in response to the cue, consistent cue conditioned dopamine signals in the DLS did not emerge (**Figure 4E**). Qualitative differences in striatal dopamine dynamics were apparent from examination of Z-scored average traces, but we also quantified several signal metrics during the first 2-sec of cue presentations that differed across regions and training phases, including the cue-evoked peak Z-score (**Figure 4F**, mixed effects ANOVA interaction of region and phase, $F(6,38)=3.14$, $p=.013$; main effect of region $F(3,21)=4.43$, $p=.015$), area under the curve (**Figure 4G**, interaction of region and phase, $F(6,38)=2.56$, $p=.035$; main effect of region, $F(3,21)=5.26$, $p=.0073$), and the rise (**Figure 4H**, interaction of region and phase, $F(6,38)=4.11$, $p=.0033$; main effect of region, $F(3,21)=4.60$, $p=.013$) and fall slopes (**Figure 4I**, interaction of region and phase, $F(6,37)=4.00$, $p=.0035$; main effect of region, $F(3,21)=3.99$, $p=.022$) of the peak signal.

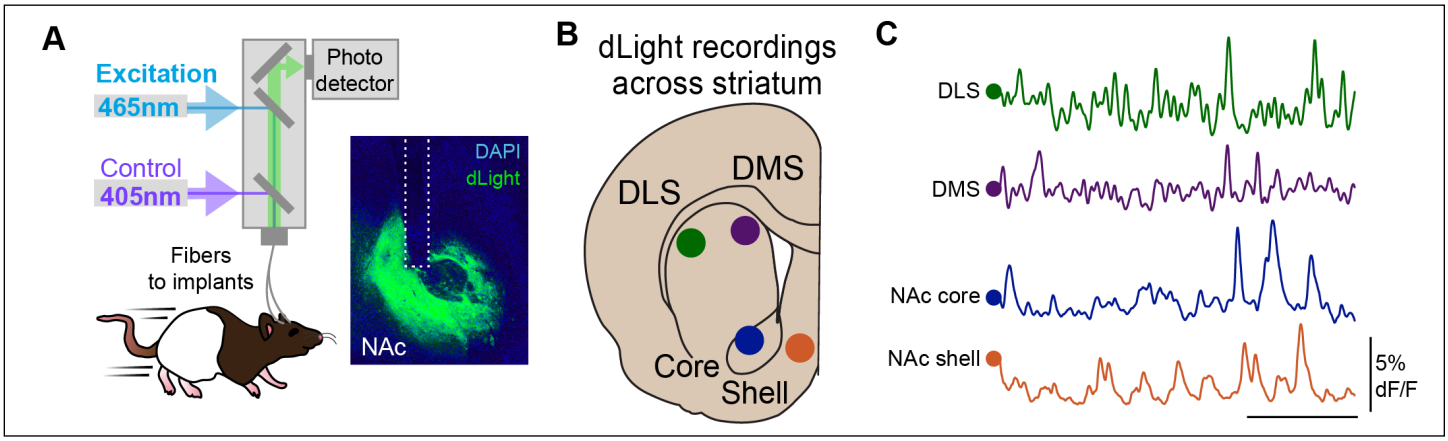

Figure 3. Recording in vivo dopamine signaling across the striatum. A) Schematic of fiber photometry system and analysis. The dopamine biosensor dLight 1.3b was expressed in the striatum of TH-cre rats expressing ChrimsonR in VTA dopamine neurons. dLight signals were fitted against an isosbestic signal, to control for photobleaching and movement artifacts. B) Photometry measurements were made from four striatal regions: the NAc medial shell (n=4), NAc core (n=6), DMS (n=6), and DLS (n=9). C) Robust spontaneous dopamine fluctuations were identified in each region.

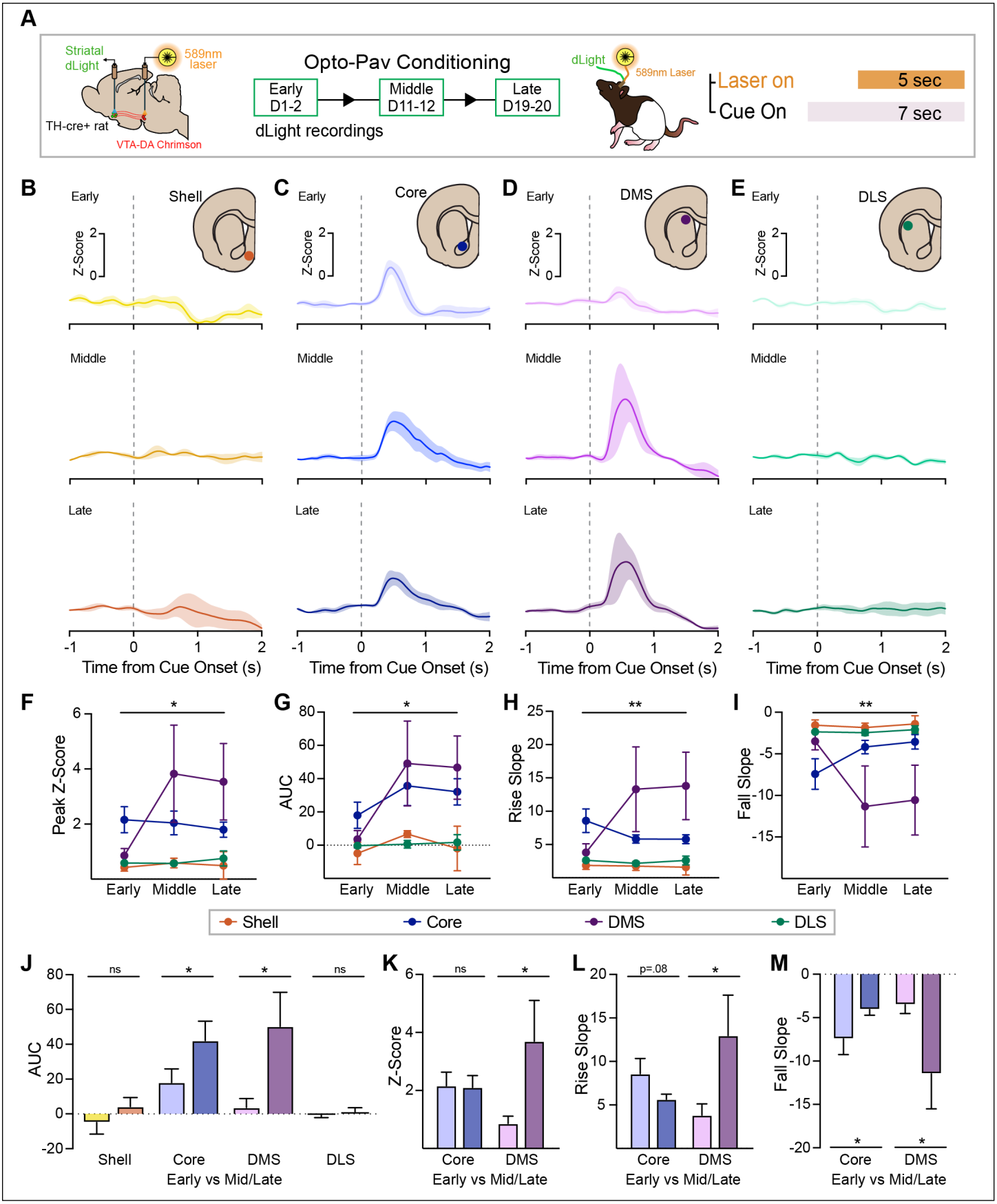

Figure 4. Spatially and temporally heterogeneous conditioned dopamine signals develop to VTA dopamine neuron predictive cues. A) Overview of recording scheme during behavioral testing. dLight signals were recorded across optogenetic Pavlovian conditioning in three training phases: early (days 1-2), middle (days 11-12), and late (days 19-20). B-E) Phasic dopamine signals in response to cues paired with optogenetic activation of VTA dopamine neurons developed only in some striatal targets. B) In the medial NAc shell, cue-evoked dopamine signals did not emerge at any training phase. C) In the NAc core, a phasic dopamine response emerged, which remained stable across training. D) In the DMS, no cue-evoked signals were present early in training, but they emerged at the middle and late phases. E) In the DLS, consistent cue-evoked signals did not emerge at any training phase.

(Figure 4 cont'd.) F-I) Cue onset-related signal dynamics, including signal peak, AUC, and the rise and fall slopes or peak signal, varied across region and training phase. J) AUC of cue-evoked signal increased in the core and DMS regions from early to later in training. K) The peak Z-score increased in the DMS but not core. L) The rise slope of the cue-evoked signal increased in the DMS. M) The fall slope of the peak signal decreased in the core and increased in the DMS. **p<.01, *p<.05.

Average NAc shell and DLS cue-related signal AUCs remained near zero and did not change across training (**Figure 4J**, paired t test for shell, t(3)=1.0, p=.39; paired t test for DLS, t(8)=.47, p=.65). In the core, while the peak Z-score (**Figure 4K**, t(5)=.09, p=.48) did not change, the AUC increased (**Figure 4J**; t(5)=2.05, p=.048) and the fall slope decreased (**Figure 4M**, t(5)=2.23, p=.038), suggesting more prolonged cue-evoked dopamine release, or a change in dopamine reuptake rate, across training. In the DMS, the AUC (**Figure 4J**, t(5)=2.55, p=.026) and peak (**Figure 4K**, t(5)=2.18, p=.04) Z-score increased between the early and middle/late training phases, suggesting dopamine signals in this region were recruited only after initial learning. The rise (**Figure 4L**, t(5)=2.34, p=.033) and fall (**Figure 4M**, t(5)=2.04, p=.048) slopes of the DMS signal also increased, suggesting an increase in the rate of dopamine release and clearance as training progressed.

We next examined the relationship between cue-evoked dopamine signals and anatomical placement of recordings sites in the striatum, independent of regional subgrouping. This revealed separate gradients spanning the medial-lateral axis in the coronal plane of the ventral versus dorsal striatum (**Supplementary Figure 6**). These gradients were opposing in their pattern and developed on different timescales. In the ventral striatum (NAc core and shell placements), cue-evoked dopamine signals were smallest in more medially positioned recording sites and became larger moving toward more lateral sites. A significant placement versus cue-evoked dLight peak signal relationship was apparent early in training (R2=.545, p=.015), and became stronger at the late training phase (R2=.613, p=.0074). In contrast, in the dorsal striatum (DMS and DLS placements), early in training there was no relationship between cue-evoked dopamine signals and anatomical placement (R2=.104, p=.24). A significant relationship developed late in training (R2=.446, p=.0065), however, where the largest cue-evoked dopamine signals were measured in medially positioned placements, which became smaller as placements moved laterally. Together this data indicates that heterogeneous cue encoding is driven by dopamine neurons, with a dynamic spatiotemporal pattern across the striatum.

VTA dopamine neuron activation evokes DA signaling preferentially in medial striatum

Optogenetic activation of VTA dopamine neurons alters neural activity in a number of downstream regions, including throughout the striatum and parts of the frontal cortex, in rodents (46,47). Here, we explored how VTA dopamine neuron activity alters dopamine signaling across the striatum (**Figure 5**). On dLight recording sessions, cues were paired with laser stimulation (20 Hz, 5 sec) on 75% of trials. Activation of VTA dopamine neurons during optogenetic conditioning produced a robust dopamine increase in the NAc medial shell, core, and DMS that was time-locked to laser delivery (**Figure 5B-E**). Focusing our analysis on the laser stimulation window, we found broadly heterogeneous dopamine signals across striatal recording sites. We quantified the average Z-score and AUC measures, which varied by region and training phase (**Figure 5F,G**; mixed effects ANOVA interaction of region and phase, F(6,38)=17.9, p<.0001); main effect of region, F(3,21)=9.11, p=.0005). In the medial shell, dopamine signals were overall largest, and increased in magnitude across training (**Figure 5B,F,G,H**; paired t test for shell, t(3)=3.01, p=.029), which was not the case for other regions. In the core (**Figure 5C,F,G,H**; paired t test for core, t(5)=.939, p=.196) and DMS (**Figure 5D,F,G,H**; paired t test for DMS, t(5)=.762, p=.24), laser-evoked dopamine signals were stable across training phases. In the DLS, we saw little laser-evoked dopamine, and this small signal actually decreased with extended training (**Figure 5E,F,G,H**; paired t test for DLS, t(8)=2.35, p=.047), despite the development of vigorous conditioned behavior. Given the large laser-evoked signal in the shell relative to the other regions, we separately analyzed signals in the core, DMS, and DLS, with the shell excluded. Stimulation-evoked dopamine remained variable across region and training phase (Interaction of phase and region, F(4,33)=4.15, p=.0078; main effect of region, F(2,18)=11.53, p=.0006). We next examined the relationship between VTA dopamine neuron stimulation and evoked dopamine signals across the sampled striatal space of our recording sites, independent of subgrouping. We found an overall gradient of laser-evoked dopamine, with the signal magnitude shrinking along the ventromedial (largest) to dorsolateral (smallest) axis in the coronal plane. Early in training, there was a trend for a correlation between recording placement in the striatum and dopamine signal (**Supplementary Figure 7**, R2=.14, p=.064), which became highly significant by the late training phase (R2=.41, p=.0005).

Dopamine signals in the NAc core and DMS, but

not shell or DLS, report dopamine prediction errors

A central feature of dopamine neuron activity is their ability to signal prediction errors, or the discrepancy between predicted and actual outcomes (12,13,48). We assessed whether striatal dopamine signals similarly report on a violation in the expectation of dopamine neuron activation (**Figure 6**). On dLight recordings sessions during optogenetic Pavlovian conditioning, 25% of trials were expectation probes, where the cue was presented normally, but laser stimulation was omitted (**Figure 6A**). Rats behaved similarly on omis-

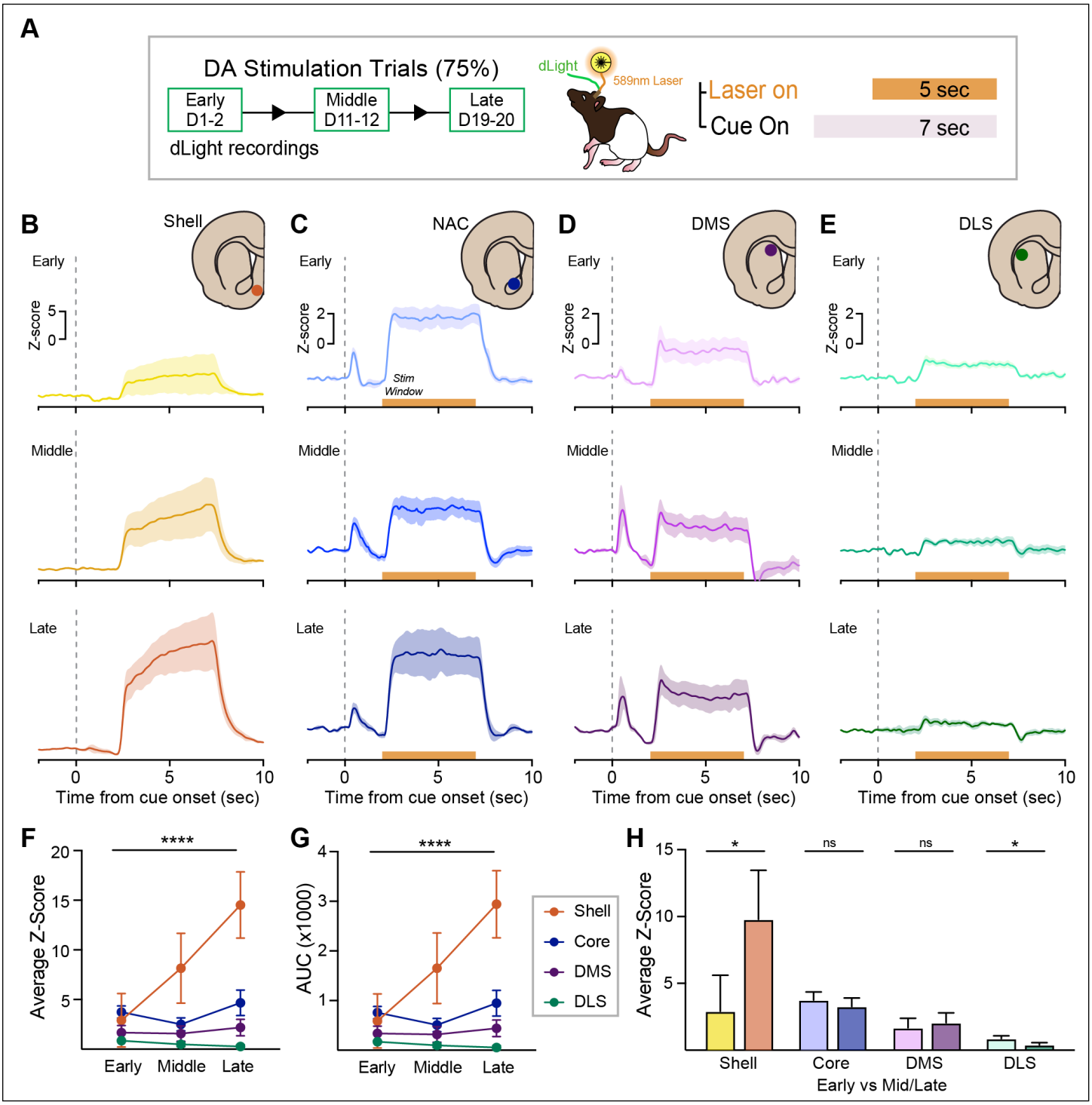

Figure 5. VTA dopamine neurons drive dopamine signaling preferentially in the medial striatum. A) Schematic of optogenetic Pavlovian conditioning paradigm. On dLight recording sessions, cues were paired with optogenetic stimulation of VTA dopamine neurons on 75% (20/25) of trials. B-C) Optogenetic activation of VTA dopamine neurons (20 Hz, 5 sec) produced different patterns of dopamine signaling across striatal targets. B) Large laser-evoked dopamine signals were present from training onset in the NAc medial shell, and this laser-evoked signal increased in magnitude across training. C) Laser evoked robust dopamine signals in the NAc core, which were stable across training. D) Laser also evoked robust dopamine signals in the DMS, which were stable across training. E) In contrast, optogenetic stimulation of VTA dopamine neurons evoked small dopamine signals in the DLS. F) Average dLight signal Z-score and G) AUC values varied significantly by region and training phase. H) Stimulation-evoked dLight signals increased in the shell, remained stable in the core and DMS, and decreased in the DLS, across training. ****p<.0001, *p<.05.

sion trials, compared to laser stimulation trials, moving in response to cues for the same percentage of time (**Figure 6B**; mixed effects ANOVA no main effect of trial type, $F(1,19)=1.81$, $p=.195$), and reaching the same maximum speed across training phases (no main effect of trial type, $F(1,19)=.748$, $p=.398$). This further underscores that behavior in our optogenetic conditioning tasks reflected learned CRs rather than simple laser-evoked movements. On omission trials, movement was tightly locked to cue-presentations (**Figure 6C**) and increased in speed and vigor across training phases (**Figure 6D-F**; average speed, $F(1.70,27.11)=23.8$, $p<.0001$; maximum speed, $F(1.54,24.61)=19.04$, $p<.0001$; time to maximum speed, $F(1.48,23.72)=61.6$, $p<.0001$), similar to stimulation trials (**Figure 1**).

We found heterogeneous signals across recording sites during these laser-omission probes (**Figure 6G-J**). Dopamine signals during the laser omission window varied as a function of region and training phase (**Figure 6K,** average Z score, mixed effects ANOVA interaction of phase and region, $F(3,21)=3.129$, $p=0.4$; **Figure 6L**, AUC, trend for interaction of phase and region, $F(3,21)=2.76$, $p=.068$, main effect of region, $F(3,21)=3.34$, $p=.039$). During the window of omission of expected dopamine neuron excitation, dopamine signals in the NAc core and DMS dipped below baseline (**Figure 6H,I**), consistent with a negative prediction error. These core and DMS error signals were not present at the beginning of training, but developed in the later phases (**Figure 6M**, paired t test for core, $t(5)=4.03$, $p=.005$; paired t test for DMS, $t(5)=2.31$, $p=.035$). This echoes dopamine responses when natural rewards are omitted (45,48,49). In contrast, dopamine signals in the shell and DLS were unresponsive to laser omission, regardless of training phase (**Figure 6G,J,M**). Taking our cue-response data (**Figure 4**) and omission data (**Figure 6**) together, we find that only the NAc core and DMS engage in prediction error-like dopamine signaling based on learning driven by VTA dopamine neuron activity.

DISCUSSION

Here, we characterized the emergence of cue-evoked behavior as a consequence of learning driven by VTA dopamine neuron activation. Recording dopamine signals with fiber photometry in four striatal regions during this optogenetic Pavlovian conditioning, we show that there is considerable regional heterogeneity in the extent that VTA dopamine neurons can drive learning-related dopamine signals downstream. In the ventral striatum, we found that cues predictive of dopamine neuron activation evoked dopamine signals first in the NAc core. In contrast, and despite VTA dopamine neuron excitation producing a robust increase in dopamine there, cue-evoked signals did not emerge in the nearby NAc medial shell. In the dorsal striatum, cue and laser-evoked dopamine signals also emerged in the DMS, with cue-evoked signals developing after NAc core signals. In contrast, extended learning mediated by VTA dopamine neuron activity was not sufficient to engage robust cue or laser-evoked dopamine signals in the DLS, despite promoting rapid conditioned movement and stereotyped behavior patterns. Finally, we found that NAc core and DMS, but not shell or DLS dopamine signals, report prediction errors by dipping in magnitude when expected dopamine neuron stimulation was omitted. Taken together, these results indicate dopamine neurons engage considerable spatial and temporal complexity in the striatum during learning. These results offer new insight into heterogeneity in striatal dopamine function, as well as the in vivo circuit architecture of the midbrain-striatum network.

Specialized cue, error, and reward signals across striatal dopamine targets

Dopamine signals in response to cues predicting optogenetic activation of VTA dopamine neurons developed specifically in the NAc core and the DMS, but on different timescales. Core signals were apparent at the beginning of conditioning, when cue-evoked movement patterns were less vigorous and more directed at the cue. Given that rats were well habituated to the cues before laser pairing began, it is unlikely that early core signals primarily reflected novelty per se (50), but perhaps instead valuation or salience of the cue that spurred approach behavior (39,51,52). Cue-evoked signals in the DMS emerged later in training, roughly in parallel to the stabilization of more rapid movement speeds and reduction in approach behavior. We also found error-related signaling in the NAc core and DMS, where dopamine signals dipped below baseline at the exact time when dopamine stimulation was omitted. In both regions, error signals only emerged after learning had occurred. The fact that this type of striatal plasticity can be engaged in the absence of learning driven by interface with a physical reward in our studies suggests that it is a fundamental feature of the system. The lack of error-related DLS dopamine fits with evidence that dopamine neuron axons in the DLS are less responsive to negative prediction errors compared to other regions (30).

Based on our data, we conclude that NAc core and DMS dopamine are unique among striatal subregions in that they prioritize encoding of expectation-related

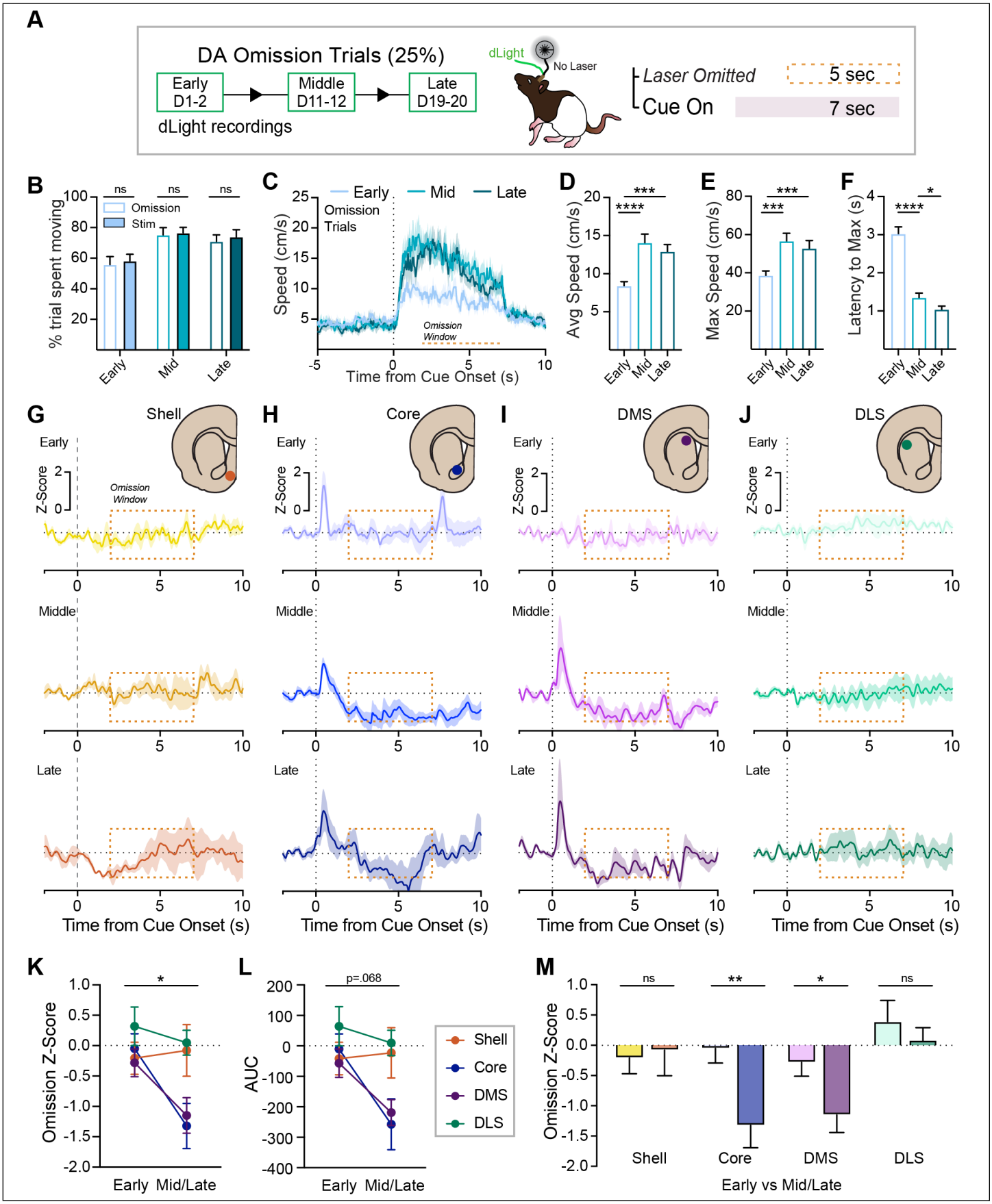

Figure 6. Dopamine signals in the NAc core and DMS, but not shell or DLS, report dopamine prediction errors. A) Schematic of optogenetic Pavlovian conditioning paradigm. On dLight recording sessions, laser delivery was omitted on 25% of cue presentations. B) Rats spent similar amounts of time moving during cue presentations on stimulation and omission trials. C) On omission trials, movement was tightly locked to cue onset and offset, increasing in speed across the early (days 1-2), middle (days 11-12), and late (days 19-20) phases of training. Both average D) and maximum E) speed achieved increased between early and middle/late training phases. F) Movement acceleration, reflected in the decreased time required to reach maximum speed, increased between each training phase. G-J) Omission of cue-paired optogenetic activation of VTA dopamine neurons led to heterogeneous dopamine

(Figure 6 cont'd.) responses across recording sites. G) Dopamine signals in the NAc medial shell did not systematically change during the laser omission window. H) In the NAc core, a laser omission-related dip in dopamine signals emerged across the middle and late training phases. I) Similarly in the DMS, omission of VTA dopamine neuron stimulation resulted in a dip in dopamine at the middle and late training phases. J) Laser omission-related changes in dopamine signal did not emerge in the DLS at any training stage. K,L) During the omission window the average signal z-score and AUC varied across region and training phase. M) Omission-related signals decreased in the core and the DMS, but not in the shell and DLS across training. ****p<.0001, ***p<.001, **p<.01, *p<.05.

information during Pavlovian learning. The broad similarity we see in NAc core and DMS dopamine signals during Pavlovian learning is interesting in light of a number of studies that show DMS and core dopamine signals diverge and have unique functional roles during instrumental decision making tasks (29,53,54). One possibility is that while nominally similar to the core, the DMS cue signals in our studies could be more related to action values and action prediction, which reflect learned cues and decision states that function somewhat independent of reward value or reinforcement (53,55–57). In other studies, major differences for the role of VTA and SNC dopamine neurons in reinforcement, cue valuation, and model-based learning are becoming clear (6,7,10,58), but direct comparisons between DMS and NAc core projecting dopamine neurons in these frameworks remain mostly undone.

Notably, we found robust VTA laser-evoked dopamine signals in the DMS, in addition to the NAc core and shell. This suggests that dopamine neurons projecting to the NAc and DMS are somewhat intermingled in the VTA/medial SNC, allowing for an interface between dopamine in the medial portion of the striatum across the dorsal-ventral axis. This idea is also supported by anatomical work (14,15). Previous studies using functional imaging to measure brain activation generated by dopamine neuron stimulation support the notion that dopamine neurons have broad access to alter network level activity (46,47). Given this, the lack of clear dopamine signals in the DLS following VTA dopamine neuron activation is perhaps surprising. It remains possible that intrinsic DLS neurons were engaged during cue or laser delivery, but it is notable that we saw a decrease in the small DLS dopamine signal generated by VTA activation. Another possibility is that DLS dopamine signals changed in some general way, porentially measurable outside of cue-trial periods on which we focused. While we did not see an increase in baseline movement speed outside of cue and laser periods across conditioning, VTA-based learning could have resulted in subtle changes in the organization of reward-independent spontaneous behavior, which is thought to engage DLS dopamine (59). Thus, DLS changes may have occurred, but not in an obvious gain-of-function capacity.

In the NAc medial shell, we found a wholly unique dopamine pattern compared to the other recording sites. There was no evidence of either cue or error-related signals in the shell, but instead, the largest laser-evoked dopamine signals. This indicates that the degree to which a striatal site can be conditioned to encode cue-related information is not simply a matter of how much dopamine is stimulated there, suggesting another component of functional specificity. Stimulation-related dopamine also increased across conditioning in the shell, in contrast to other sites. This suggests unique mechanisms regulate dopamine release in the shell during learning, potentially at the terminal level (60). Recent evidence also indicates anatomically localized functions for the shell are partly due to the specific patterns of connectivity with the midbrain (33,61), compared to other parts of the ventral striatum. Overall our results fit with the general notion that dopamine in the medial shell preferentially signals reward and reward value over other features of learning (62–65). They also support anatomical frameworks classifying the medial shell as part of a distinct brain macrosystem within limbic networks (66,67).

Implications for the functional architecture of the midbrain-striatum network

The unique nature of our study, where we isolated the impact of learning driven directly by VTA dopamine neurons, allows determination of how VTA dopamine neurons engage the broader striatal network, for insight on long-standing questions about its functional organization. In the classic ascending spiral framework (16,17), behavioral control and neural signals transition from VTA inputs to the ventral striatum to SNC inputs to the dorsal striatum (18–20) in parallel with stereotyped, habitual action patterns seen after extended learning (21). Our results potentially offer some support for this, given that conditioned dopamine signaling engaged by VTA dopamine neuron mediated learning first appeared in the NAc, then later emerged in the DMS, when conditioned behavior was more vigorous. Critically, we show that rather than a shift away from ventral striatum, an additive, progressive recruitment of dorsal striatum occurs instead. This recruitment also appears to be limited to medial dorsal regions, as we did not see DLS dopamine activity emerge.

Overall our work fits with recent ex vivo work demonstrating that, contrary to the spiral hypothesis, DMS-projecting dopamine neurons do not have circuit-level functional connectivity with DLS-projecting dopamine neurons (68). Rather, midbrain-striatal systems exist

as reciprocal, parallel, primarily independent loops, where VTA dopamine neurons can control their own (but not SNC) activity via direct pathway projections from the ventral striatum (17,61,68–70). This suggests that at least in naive mice, there is no circuit connectivity to support an ascending DLS engagement, but a critical component of the spiral framework is that learning-mediated plasticity recruits a spiral mechanism. Our work tests this notion in vivo, and we find little direct evidence: despite extended Pavlovian learning via VTA dopamine neuron activation that produces rapid cue-evoked movement patterns, neither cue nor robust laser-evoked dopamine signals emerge in the DLS. Consistent with this, NAc, but not DLS dopamine signaling and neural activity remain important for normal execution of Pavlovian conditioned cue approach after extended training (28). The type of learning framework is likely key for how striatal networks are engaged, but this is not restricted to Pavlovian learning, as other recent work highlights a lack of a shift toward DLS dopamine signals and striatal activity during the development of outcome-insensitive instrumental habits (24–26). Collectively, our data support an updated account of the functional architecture of midbrain-striatal loops, where learning is not predicated on a consistent shift from the ventromedial to dorsolateral axis in either dopamine signaling or striatal activity.

It is important to consider our current results in the context of seminal studies clearly demonstrating a shift in striatal recruitment to DLS (19,20,71,72). The strongest evidence for this effect comes from instrumental conditioning studies where cocaine is self administered for extended periods. This suggests that chronic hyperactivation of the dopamine system via drug stimuli may be necessary to promote DLS recruitment. Actual commerce with an external reward is not essential, however, as dopamine neuron self stimulation can promote plasticity in corticostriatal neurons that is similar to that produced by cocaine self administration, independent of other reward exposure (73,74). Thus, DLS recruitment may depend on whether mesolimbic dopamine circuits are activated in a rapid, binge-like, or escalating fashion. Another possibility in our studies is that the DLS was conditionally recruited via mechanisms that are not reported by changes in dopamine release, including potentiation of corticostriatal inputs (75,76). Recent efforts have also characterized functionally distinct roles for striatal output pathways in behavioral control, via parallel channels through the thalamus, midbrain, and cortex (70,77,78). It will be important to investigate how dopamine neuron activity may engage such broader nigro-thalamo-cortical and striatal loops, which could provide a circuit mechanism by which midbrain inputs to the ventral striatum can engage dorsal striatum, independent of the classic spiral mechanisms. The recent discovery of pan-striatal wave-like activation patterns among dopamine signals and cholinergic interneurons provides another possible source of ventral-dorsal interactions (79,80).

Conclusions

Here, by measuring dopamine signals and behavior emergent from learning driven by VTA dopamine neurons in the absence of other rewards, we uncover fundamental, region-specific patterns of dopamine signaling engaged during Pavlovian learning. Our results show that VTA dopamine neurons direct learning about environmental cues by driving broad plasticity in the dopamine system, where preferential reward, cue, and error-related signaling in subregions of the ventral and dorsal striatum develop across learning phases. This work provides new insight into the functional architecture of the striatal network, building on long-standing anatomical and in vivo recording frameworks positing a shift in striatal control to the dorsal striatum as learning progresses. We find that dopamine neurons do not drive such a shift, despite the development of vigorous, cue-controlled movement patterns. Instead, as learning progresses, a broader landscaping of dopamine release patterns emerges across a network of ventral and dorsal striatal targets to uniquely encode reward and prediction-related features of learning.

METHODS

Subjects

Male and female TH-cre transgenic rats (n=20; 12 F, 8 M) bred on a Long-Evans background were used. These rats express Cre recombinase under the control of the tyrosine hydroxylase (TH) promoter (40). All rats weighed 250-500g at the time of surgery and were 4-7 months old at the time of experimentation. Experimental procedures were approved by the Institutional Animal Care and Use Committee at the University of Minnesota and were carried out in accordance with the guidelines on animal care and use of the National Institutes of Health of the United States.

Surgical Procedures

Rats were anesthetized with 5% isoflurane and placed in a stereotaxic frame, after which anesthesia was maintained at 1-3%. Rats were administered saline, carprofen anesthetic (5 mg/kg), and cefazolin antibiotic (70 mg/kg) subcutaneously prior to start of surgery. The top of the skull was exposed and holes were made for viral infusion needles, optic fiber implants, and 4 skull

screws. A total of 1.2 µL of virus (pAAV5-Syn-FLEX-Chrimson-tdTomato, Addgene) was infused unilaterally into the VTA (-6.0 AP, +/- 0.7 ML, -8.0 DV). In the same hemisphere, a virus coding for the dopamine biosensor dLight 36 (AAV5-hSyn-dLight1.3b, University of Minnesota Viral Vector and Cloning Core) was infused into the NAc (1.3 AP, +/- 1.3 ML, -7.0 DV), DMS (1.3 AP, +/- 1.3 ML, -4.3 DV), or DLS (1.7 AP, +/- 4.0 ML, -5.0 DV) at a total volume of 0.8 µL. All viruses were delivered at 0.1µL/min. Immediately after injection, the needle was raised 100 µm and then left in place for an additional 10 min to allow for diffusion. Optical fibers (9mm length, 400µm diameter, Doric Lenses) for photometry recordings were chronically implanted into the NAc (1.3 AP, +/- 1.3 ML, -6.6 DV), DMS (1.3 AP , +/- 1.3 ML, -4.3 DV), or dorsal striatum (1.7 AP, +/- 4.0 ML, -4.4 DV), and optic fibers (10mm length, 200µm diameter, Thorlabs) for optogenetic stimulation were implanted above the VTA (-6.0 AP, +/- 0.7 ML, -7.9 DV) in the same hemisphere as the viral infusions (**Supplemental Figure 1**). All coordinates are in mm relative to bregma and skull surface. Implants were secured to the skull with dental acrylic (Lang Dental) applied around the skull screws and the base of the ferrules containing the optic fibers. At the end of all surgeries, topical anesthetic and antibiotic ointment were applied to the surgical site, rats were placed on a heating pad and monitored until they were ambulatory. After surgery rats were individually housed with ad libitum access to food and water on a 0800 to 2000 light/dark cycle (lights on at 0800), given carprofen (5 mg/kg) and cefazolin (70 mg/kg) for the first 3 days following surgery and weighed and monitored for 6 days. Optogenetic manipulations commenced at least 4 weeks after surgery. Post hoc validation of optic fiber placements revealed subsets of rats with fibers targeted to the core versus medial shell of the NAc, which we analyzed separately.

Optogenetic Stimulation

Optogenetics studies used 589 nm lasers (OptoEngine and Dragon Lasers). Light output during individual 5-ms light pulses during experiments was adjusted to be approximately 2 mW/mm2 at the tip of the intracranial fiber. For all optogenetic studies, optic tethers connecting rats to the rotary joint were sheathed in a lightweight armored jacket to prevent cable breakage and block visible light transmission. Laser pulses were initiated from Med-PC TTL pulses and patterned via Synapse software that also controlled photometry and video data acquisition.

Fiber Photometry

To assess dopamine signaling across the striatum during Pavlovian conditioning, we measured dLight fluorescence in the NAc core, NAc shell, DMS, and DLS using fiber photometry (**Figures 3-6**; **Supplemental Figures 3-7**). A fluorescence mini-cube (Doric-Lenses) transmitted light streams from 465 nm and 405 nm LEDs (Doric-Lenses), sinusoidally modulated at 211 Hz, and 330 Hz, respectively. LED power was set at ~100 µW. On recording days rats were tethered to a core, shell, DMS, or DLS implant using a low autofluorescence cable sheathed in a lightweight armored jacket (Doric-Lenses). On all photometry recording days the rats were simultaneously tethered to the VTA implant as described above. Photometry recordings were conducted on specific days with interspersed recording free days (No recording days: 3, 6, 9-10, 13-14, and 17-18). Recording data here are sampled from the early (day 1 and 2), middle (day 11 and 12) and late (day 19 and 20) stages of Pavlovian conditioning.

Fluorescence from below the fiber tip was transmitted back to the mini cube, where it was passed through a GFP emission filter, amplified, and focused onto a high sensitivity photoreceiver (Newport, Model 2151). A real-time signal processor (RZ5P, Tucker Davis Technologies) running Synapse software modulated the output of each LED and recorded photometry signals, which were sampled from the photodetector at 6.1 kHz. Demodulation of the brightness produced by the 465-nm excitation, which stimulates dopamine-dependent dLight fluorescence, versus isosbestic 405-nm excitation, which stimulates dLight in a dopamine-independent manner, allowed for correction for bleaching and movement artifacts. Task events (e.g., cue and laser presentations), were time stamped in the photometry data file via a TTL signal from the Med-PC behavioral program, and behavior was video recorded as described below at 10-20 FPS, with timestamps for each frame captured in the photometry file.

Habituation and Optogenetic Pavlovian Training

Optogenetic Pavlovian training was conducted as described previously 6. Briefly, rats were first acclimated to the behavioral chambers (Med Associates), conditioning cues, and optic cable tethering in a ~30-min habituation session. During this session, rats were tethered to a rotary joint and 20 cue presentations, with no other consequences, were presented on a 90-s average variable time (VT) schedule. In each of the subsequent conditioning sessions, rats were presented with 20 cue (light + tone, 7 s) – laser stimulation (100 5-ms pulses at 20 Hz; laser train initiated 2 s after cue onset and continued for duration of cue) pairings delivered on a 100-sec VT schedule as well as 5 cue presentations with no laser pairings, serving as probe trials,

randomly distributed across the session. The sessions lasted ~42 min. These cues were never associated with another external stimulus (e.g., food or water). Cue and laser delivery were never contingent on an animal's behavior and all rats received the same number of cue and laser events. On photometry recording days, 25% (5/25, randomly delivered) of trials served as dopamine omission probes, wherein cues were presented as normal, but laser stimulation did not occur.

Video Scoring

During Pavlovian conditioning sessions behavior was video recorded using cameras (Vanxse CCTV Security Camera) positioned a standardized distance above each chamber. Videos from sessions 1, 2, 4, 8, 11, 12, and 19, 20 were scored offline by observers who were blind to the identity and anatomical target group of the rats. For days 1, 4, 8, 12, and 20, each cue-only (2-sec, 25 per session) and cue+laser (5-sec, 20 per session) event was scored for the occurrence and onset latency of the following behaviors. Locomotion: Defined as the rat moving all four feet in a forward direction (i.e., not simply lifting feet in place). Cue Approach: Defined as the rat's nose coming within 2.5 cm of the cue light. Approach often involved the rat moving from another area of the chamber to come in physical contact with the cue light while it was illuminated. Rearing: Defined as the rat lifting its head and front feet off the chamber floor, either onto the side of the chamber, or into the air. Rotation: Defined as the rat making a complete 360-degree turn in one direction. For cue approach and rotation, the number of occurrences were also scored. For days 2, 11, and 19, only locomotion was scored.

DeepLabCut pose estimation

Markerless tracking of animal body parts was conducted using version 2.2.1.1 of the DeepLabCut (DLC) Toolbox 37,41 and analysis of movement features based on these tracked coordinates was conducted in Matlab R2020b (Mathworks). All DLC analysis was conducted on a Dell G7-7590 laptop running Windows 10 with an Intel Core i7-9750H CPU, 2.60Ghz, 16 GB RAM, and an NVIDIA GeForce RTX 2080 Max-Q 8GB GPU. DeepLabCut 2.2.1.1 was installed in an Anaconda environment with Python 3.8.4, CUDA 11.7 and Tensorflow 2.10.

DeepLabCut Model: 2090 frames from 35 videos (32 different animals, 3 experiments) were labeled and 807 outlier frames were relabelled to refine the network. Labeled frames were split into a training set (95% of frames) and a test set (5% of frames). A ResNet-50 based neural network 42 was used for 1,030,000 training iterations. After the final refinement we found the test error was 4.1 pixels, the training error was 3.13 pixels and with a p-cutoff of 0.85 training error was 2.99 pixels and test error was 3.68 pixels. The body parts labeled included the nose, eyes, ears, center of head or fiber optic implant, shoulders, tail base, and an additional three points along the spine. Features of the environment were also labeled, including the 4 corners of the apparatus floor, two nose ports, two cue lights, two magazine ports, and 3 LED indicator lights when active (see **Supplemental Figure 2** for examples of labeled body parts and environment features).

Behavior Analysis: DLC coordinates and confidence values for each bodypart and frame were imported to Matlab and filtered to exclude body parts/features from any frame where the confidence was < 0.7. For labeled features of the environment, which have a fixed location, the average coordinates for that recording were used for analysis. To convert pixel distances to the real chamber dimensions, for each video, a pixel to cm conversion rate was determined. The distance (in pixels) between each edge of the environment floor and the diagonal measurements from corner to corner was measured, and these values were divided by the actual distance in cm. The mean of these values was then used as the conversion factor. Movement speed was calculated from the implant coordinates frame by frame using the formula: [distance moved (pix per cm) * framerate] to give movement speed in cm/s. For plotting of speed data across recordings with different sampling rates, missing data points for the lower sampling rate sessions were filled in using linear interpolation with the interpol1 function (MATLAB), interpolated data points were not used to calculate peak or mean speeds for analysis. Approach to the cue light was detected by finding frames in which the nose was within 2.5 cm from the cue. The beginning and end of each approach occurred when the nose was further than 4.5 cm from the cue for 0.2s. Only approaches longer than 0.2 s were considered. The latency to approach and time spent approaching during the cue presentation were calculated for each trial. Locomotion was detected using the speed of the 4 positions on the spine to detect whole-body movements. The movement threshold for detecting locomotion was calibrated to animal size using a scale factor determined from the relationship between body size (distance between the shoulder and mid-back points) and the optimal threshold for detecting movement in a separate group of animals not used for this study (n = 4). Locomotion bouts were detected when all of the visible body parts were above the movement threshold and a sliding window was used to determine when the speed of 2 or more body parts reached less than 50% of the detection threshold for

0.3s, indicating the beginning and end of a movement. Movements less than 0.5s in duration were excluded. Latency to begin moving and total duration of movement time were calculated for each trial. Orientation toward the cue light was determined by calculating the angle between the vector from the implant to the nose with the vector from the implant to the cue. Animals were considered oriented to the cue whenever this angle was < 30° for more than 0.2s. Latency to orient to the cue, and time spent orienting during cue presentation were calculated.

Photometry data collection and analysis

Photometry data was analyzed using a custom MATLAB pipeline. For analysis, signals were filtered with a 2 Hz lowpass filter, downsampled to 40 Hz, and a least-squares linear fit was applied to the 405-nm signal, to align it to the 465-nm signal (Supplementary Figure 4). This fitted 405-nm signal was used to normalize the 465-nm signal, where ΔF/F = (465-nm signal – fitted 405-nm signal)/(fitted 405-nm signal). Normalized signals for each trial were extracted for 5s before and 10s after each cue presentation and Z-scored to the 5s pre-cue period for each trial to minimize the effects of drift in the signal across experiment duration. Cue responses were detected in the average trial waveform for each animal in the 2s window beginning at cue onset (and prior to optogenetic stimulation). Responses to the presence or absence of optogenetic stimulation were detected in the average trial waveforms for each animal across the 5s stimulation window, beginning 2s after cue onset. The maximum and minimum responses in each window were detected and latency was calculated relative to the start of the detection window. The slope of the rising and falling phase of the peak and trough waveforms were calculated between the maximum and 50% of max using the formula t2-t1/f2-f1, where t is the beginning and end timepoints of the rising or falling phase of the waveform, and f is the z-scored fluorescence at each timepoint. In some cases, the values did not drop below 50% of max in the available window, in these instances the minimum value between the max and beginning or end of the window were used instead. Area under the curve (AUC) values were calculated from the z-scored traces by numerical integration via the trapezoidal method using the trapz function (MATLAB). AUC of cue responses was calculated over the first 1s post-cue. AUC for the stimulation window was calculated over the entire 5-sec optogenetic stimulation window. Recording groups were as follows **(Supplementary Figure 5**): NAc shell (n=4), NAc core (n=6), DMS (n=6), and DLS (n=9).

Statistics

Behavior and photometry signal data were analyzed with a combination of linear mixed-effects ANOVA models, planned t tests, and Pearson correlations. Graphs represent averages of recordings sites/subjects, not individual trials. The data are expressed as the mean ± s.e.m. Statistical significance was set at $p<0.05$.

Histology

Rats were deeply anesthetized with sodium pentobarbital (2 mL/kg) and transcardially perfused with cold phosphate buffered saline followed by 4% paraformaldehyde. Brains were removed and post-fixed in 4% paraformaldehyde for ~24 hours, then cryoprotected in a 25% sucrose solution for at least 48 hours. Sections were cut at 50 microns on a cryostat (Leica CM1900). To confirm viral expression and optic fiber placements, brain sections containing the midbrain were mounted on microscope slides and coverslipped with Vectashield containing DAPI counterstain. Fluorescence from Chrimson and dLight as well as optic fiber damage location was then visualized.

REFERENCES

1. Berke, J. D. What does dopamine mean? Nat. Neurosci. 21, 787–793 (2018).
2. Keiflin, R. & Janak, P. H. Dopamine prediction errors in reward learning and addiction: from theory to neural circuitry. Neuron 88, 247–263 (2015).
3. Schultz, W. Behavioral theories and the neurophysiology of reward. Annu. Rev. Psychol. 57, 87–115 (2006).
4. Cox, J. & Witten, I. B. Striatal circuits for reward learning and decision-making. Nat. Rev. Neurosci. 20, 482–494 (2019).
5. Robinson, T. E. & Berridge, K. C. The neural basis of drug craving: an incentive-sensitization theory of addiction. Brain Res. Brain Res. Rev. 18, 247–291 (1993).
6. Saunders, B. T., Richard, J. M., Margolis, E. B. & Janak, P. H. Dopamine neurons create Pavlovian conditioned stimuli with circuit-defined motivational properties. Nat. Neurosci. 21, 1072–1083 (2018).
7. Sharpe, M. J. et al. Dopamine transients are sufficient and necessary for acquisition of model-based associations. Nat. Neurosci. 20, 735–742 (2017).
8. Howe, M. W. & Dombeck, D. A. Rapid signalling in distinct dopaminergic axons during locomotion and reward. Nature 535, 505–510 (2016).
9. Tsai, H.-C. et al. Phasic firing in dopaminergic neurons is sufficient for behavioral conditioning. Science 324, 1080–1084 (2009).
10. Keiflin, R., Pribut, H. J., Shah, N. B. & Janak, P. H. Ventral tegmental dopamine neurons participate in reward identity predictions. Curr. Biol. 29, 93-103.e3 (2019).
11. Steinberg, E. E. et al. A causal link between prediction errors, dopamine neurons and learning. Nat. Neurosci. 16, 966–973 (2013).
12. Cohen, J. Y., Haesler, S., Vong, L., Lowell, B. B. &

Uchida, N. Neuron-type-specific signals for reward and punishment in the ventral tegmental area. Nature 482, 85–88 (2012).
13. Schultz, W., Dayan, P. & Montague, P. R. A neural substrate of prediction and reward. Science 275, 1593–1599 (1997).
14. Breton, J. M. et al. Relative contributions and mapping of ventral tegmental area dopamine and GABA neurons by projection target in the rat. J. Comp. Neurol. 527, 916–941 (2019).
15. Swanson, L. W. The projections of the ventral tegmental area and adjacent regions: a combined fluorescent retrograde tracer and immunofluorescence study in the rat. Brain Res. Bull. 9, 321–353 (1982).
16. Haber, S. N., Fudge, J. L. & McFarland, N. R. Striatonigrostriatal pathways in primates form an ascending spiral from the shell to the dorsolateral striatum. J. Neurosci. 20, 2369–2382 (2000).
17. Lerner, T. N. Interfacing behavioral and neural circuit models for habit formation. J. Neurosci. Res. 98, 1031–1045 (2020).
18. Belin, D. & Everitt, B. J. Cocaine seeking habits depend upon dopamine-dependent serial connectivity linking the ventral with the dorsal striatum. Neuron 57, 432–441 (2008).
19. Willuhn, I., Burgeno, L. M., Everitt, B. J. & Phillips, P. E. M. Hierarchical recruitment of phasic dopamine signaling in the striatum during the progression of cocaine use. Proc Natl Acad Sci USA 109, 20703–20708 (2012).
20. Porrino, L. J., Lyons, D., Smith, H. R., Daunais, J. B. & Nader, M. A. Cocaine self-administration produces a progressive involvement of limbic, association, and sensorimotor striatal domains. J. Neurosci. 24, 3554–3562 (2004).
21. Yin, H. H. & Knowlton, B. J. The role of the basal ganglia in habit formation. Nat. Rev. Neurosci. 7, 464–476 (2006).
22. Everitt, B. J. & Robbins, T. W. Neural systems of reinforcement for drug addiction: from actions to habits to compulsion. Nat. Neurosci. 8, 1481–1489 (2005).
23. Lüscher, C. & Janak, P. H. Consolidating the circuit model for addiction. Annu. Rev. Neurosci. 44, 173–195 (2021).
24. Seiler, J. L. et al. Dopamine signaling in the dorsomedial striatum promotes compulsive behavior. Curr. Biol. 32, 1175-1188.e5 (2022).
25. Vandaele, Y. et al. Distinct recruitment of dorsomedial and dorsolateral striatum erodes with extended training. eLife 8, (2019).
26. van Elzelingen, W. et al. Striatal dopamine signals are region specific and temporally stable across action-sequence habit formation. Curr. Biol. 32, 1163-1174.e6 (2022).
27. Coddington, L. T. & Dudman, J. T. The timing of action determines reward prediction signals in identified midbrain dopamine neurons. Nat. Neurosci. 21, 1563–1573 (2018).
28. Fraser, K. M. & Janak, P. H. Long-lasting contribution of dopamine in the nucleus accumbens core, but not dorsal lateral striatum, to sign-tracking. Eur. J. Neurosci. 46, 2047–2055 (2017).
29. Parker, N. F. et al. Reward and choice encoding in terminals of midbrain dopamine neurons depends on striatal target. Nat. Neurosci. 19, 845–854 (2016).
30. Tsutsui-Kimura, I. et al. Distinct temporal difference error signals in dopamine axons in three regions of the striatum in a decision-making task. eLife 9, (2020).
31. Brown, H. D., McCutcheon, J. E., Cone, J. J., Ragozzino, M. E. & Roitman, M. F. Primary food reward and reward-predictive stimuli evoke different patterns of phasic dopamine signaling throughout the striatum. Eur. J. Neurosci. 34, 1997–2006 (2011).
32. Liu, Y. et al. The Mesolimbic Dopamine Activity Signatures of Relapse to Alcohol-Seeking. J. Neurosci. 40, 6409–6427 (2020).
33. de Jong, J. W. et al. A neural circuit mechanism for encoding aversive stimuli in the mesolimbic dopamine system. Neuron 101, 133-151.e7 (2019).
34. Collins, A. L. & Saunders, B. T. Heterogeneity in striatal dopamine circuits: Form and function in dynamic reward seeking. J. Neurosci. Res. 98, 1046–1069 (2020).
35. Mohebi, A. et al. Dissociable dopamine dynamics for learning and motivation. Nature 570, 65–70 (2019).
36. Patriarchi, T. et al. Ultrafast neuronal imaging of dopamine dynamics with designed genetically encoded sensors. Science 360, (2018).
37. Mathis, A. et al. DeepLabCut: markerless pose estimation of user-defined body parts with deep learning. Nat. Neurosci. 21, 1281–1289 (2018).
38. Saunders, B. T. & Robinson, T. E. The role of dopamine in the accumbens core in the expression of Pavlovian-conditioned responses. Eur. J. Neurosci. 36, 2521–2532 (2012).
39. Flagel, S. B. et al. A selective role for dopamine in stimulus-reward learning. Nature 469, 53–57 (2011).
40. Witten, I. B. et al. Recombinase-driver rat lines: tools, techniques, and optogenetic application to dopamine-mediated reinforcement. Neuron 72, 721–733 (2011).
41. Nath, T. et al. Using DeepLabCut for 3D markerless pose estimation across species and behaviors. Nat. Protoc. 14, 2152–2176 (2019).
42. Insafutdinov, E., Pishchulin, L., Andres, B., Andriluka, M. & Schiele, B. DeeperCut: A Deeper, Stronger, and Faster Multi-person Pose Estimation Model. in Computer vision – ECCV 2016 (eds. Leibe, B., Matas, J., Sebe, N. & Welling, M.) vol. 9910 34–50 (Springer International Publishing, 2016).3. Lee, K. et al. Temporally restricted dopaminergic control of reward-conditioned movements. Nat. Neurosci. 23, 209–216 (2020).
43. Lee, K. et al. Temporally restricted dopaminergic control of reward-conditioned movements. Nat. Neurosci. 23, 209–216 (2020).
44. Flagel, S. B., Akil, H. & Robinson, T. E. Individual differences in the attribution of incentive salience to reward-related cues: Implications for addiction. Neuropharmacology 56 Suppl 1, 139–148 (2009).
45. Day, J. J., Roitman, M. F., Wightman, R. M. & Carelli, R.

M. Associative learning mediates dynamic shifts in dopamine signaling in the nucleus accumbens. Nat. Neurosci. 10, 1020–1028 (2007).
46. Decot, H. K. et al. Coordination of Brain-Wide Activity Dynamics by Dopaminergic Neurons. Neuropsychopharmacology 42, 615–627 (2017).
47. Lohani, S., Poplawsky, A. J., Kim, S. G. & Moghaddam, B. Unexpected global impact of VTA dopamine neuron activation as measured by opto-fMRI. Mol. Psychiatry 22, 585–594 (2017).
48. Waelti, P., Dickinson, A. & Schultz, W. Dopamine responses comply with basic assumptions of formal learning theory. Nature 412, 43–48 (2001).
49. Eshel, N. et al. Arithmetic and local circuitry underlying dopamine prediction errors. Nature 525, 243–246 (2015).
50. Kutlu, M. G. et al. Dopamine signaling in the nucleus accumbens core mediates latent inhibition. Nat. Neurosci. 25, 1071–1081 (2022).
51. Berridge, K. C. The debate over dopamine's role in reward: the case for incentive salience. Psychopharmacology (Berl) 191, 391–431 (2007).
52. Wassum, K. M., Ostlund, S. B., Loewinger, G. C. & Maidment, N. T. Phasic mesolimbic dopamine release tracks reward seeking during expression of Pavlovian-to-instrumental transfer. Biol. Psychiatry 73, 747–755 (2013).
53. Lee, R. S., Mattar, M. G., Parker, N. F., Witten, I. B. & Daw, N. D. Reward prediction error does not explain movement selectivity in DMS-projecting dopamine neurons. eLife 8, (2019).
54. Moss, M. M., Zatka-Haas, P., Harris, K. D., Carandini, M. & Lak, A. Dopamine axons in dorsal striatum encode contralateral visual stimuli and choices. J. Neurosci. 41, 7197–7205 (2021).
55. Hollon, N. G. et al. Nigrostriatal dopamine signals sequence-specific action-outcome prediction errors. Curr. Biol. 31, 5350-5363.e5 (2021).
56. Coddington, L. T. & Dudman, J. T. Learning from Action: Reconsidering Movement Signaling in Midbrain Dopamine Neuron Activity. Neuron 104, 63–77 (2019).
57. Howard, C. D., Li, H., Geddes, C. E. & Jin, X. Dynamic nigrostriatal dopamine biases action selection. Neuron 93, 1436-1450.e8 (2017).
58. Fraser, K. M., Pribut, H. J., Janak, P. H. & Keiflin, R. From prediction to action: dissociable roles of ventral tegmental area and substantia nigra dopamine neurons in instrumental reinforcement. J. Neurosci. (2023) doi:10.1523/JNEUROSCI.0028-23.2023.
59. Markowitz, J. E. et al. Spontaneous behaviour is structured by reinforcement without explicit reward. Nature 614, 108–117 (2023).
60. Cachope, R. & Cheer, J. F. Local control of striatal dopamine release. Front. Behav. Neurosci. 8, 188 (2014).
61. Yang, H. et al. Nucleus accumbens subnuclei regulate motivated behavior via direct inhibition and disinhibition of VTA dopamine subpopulations. Neuron 97, 434-449.e4 (2018).
62. Di Chiara, G. Nucleus accumbens shell and core dopamine: differential role in behavior and addiction. Behav. Brain Res. 137, 75–114 (2002).
63. Beyene, M., Carelli, R. M. & Wightman, R. M. Cue-evoked dopamine release in the nucleus accumbens shell tracks reinforcer magnitude during intracranial self-stimulation. Neuroscience 169, 1682–1688 (2010).
64. Sackett, D. A., Saddoris, M. P. & Carelli, R. M. Nucleus accumbens shell dopamine preferentially tracks information related to outcome value of reward. eNeuro 4, (2017).
65. Saddoris, M. P., Cacciapaglia, F., Wightman, R. M. & Carelli, R. M. Differential dopamine release dynamics in the nucleus accumbens core and shell reveal complementary signals for error prediction and incentive motivation. J. Neurosci. 35, 11572–11582 (2015).
66. Zahm, D. S. & Brog, J. S. On the significance of subterritories in the "accumbens" part of the rat ventral striatum. Neuroscience 50, 751–767 (1992).
67. Swanson, L. W. Anatomy of the soul as reflected in the cerebral hemispheres: neural circuits underlying voluntary control of basic motivated behaviors. J. Comp. Neurol. 493, 122–131 (2005).
68. Ambrosi, P. & Lerner, T. N. Striatonigrostriatal circuit architecture for disinhibition of dopamine signaling. Cell Rep. 40, 111228 (2022).
69. Lerner, T. N. et al. Intact-Brain Analyses Reveal Distinct Information Carried by SNc Dopamine Subcircuits. Cell 162, 635–647 (2015).
70. Lee, J., Wang, W. & Sabatini, B. L. Anatomically segregated basal ganglia pathways allow parallel behavioral modulation. Nature Neuroscience (2020).
71. Willuhn, I., Burgeno, L. M., Groblewski, P. A. & Phillips, P. E. M. Excessive cocaine use results from decreased phasic dopamine signaling in the striatum. Nat. Neurosci. 17, 704–709 (2014).
72. Clark, J. J., Collins, A. L., Sanford, C. A. & Phillips, P. E. M. Dopamine encoding of Pavlovian incentive stimuli diminishes with extended training. J. Neurosci. 33, 3526–3532 (2013).
73. Pascoli, V. et al. Stochastic synaptic plasticity underlying compulsion in a model of addiction. Nature 564, 366–371 (2018).
74. Pascoli, V., Terrier, J., Hiver, A. & Lüscher, C. Sufficiency of mesolimbic dopamine neuron stimulation for the progression to addiction. Neuron 88, 1054–1066 (2015).
75. Rothwell, P. E. et al. Input- and Output-Specific Regulation of Serial Order Performance by Corticostriatal Circuits. Neuron 88, 345–356 (2015).
76. Poldrack, R. A. et al. The neural correlates of motor skill automaticity. J. Neurosci. 25, 5356–5364 (2005).
77. Lee, J. & Sabatini, B. L. Striatal indirect pathway mediates action switching via modulation of collicular dynamics. BioRxiv (2020) doi:10.1101/2020.10.01.319574.
78. Aoki, S. et al. An open cortico-basal ganglia loop allows limbic control over motor output via the nigrothalamic pathway. eLife 8, (2019).
79. Hamid, A. A., Frank, M. J. & Moore, C. I. Wave-like dopamine dynamics as a mechanism for spatiotemporal credit assignment. Cell 184, 2733-2749.e16 (2021).
80. Rehani, R. et al. Activity patterns in the neuropil of striatal cholinergic interneurons in freely moving mice represent their collective spiking dynamics. eNeuro 6, (2019).

Supplemental Figures

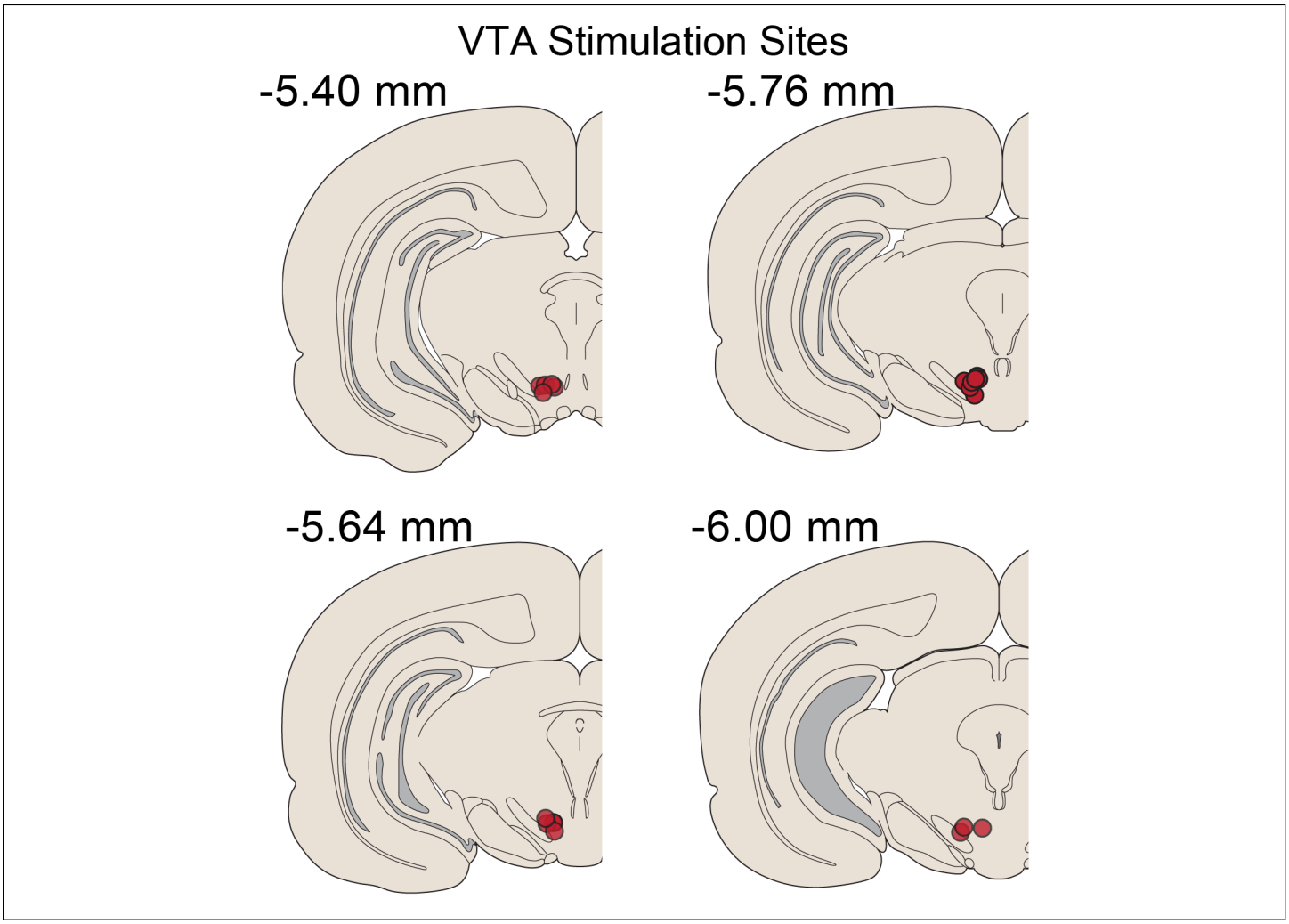

Supplementary Figure 1. Coronal atlas plates showing location of the tips of fiber optic implants for targeting optogenetic stimulation to dopamine neurons in the ventral tegmental area (VTA) in TH-cre rats. Coordinates are in mm with respect to Bregma.

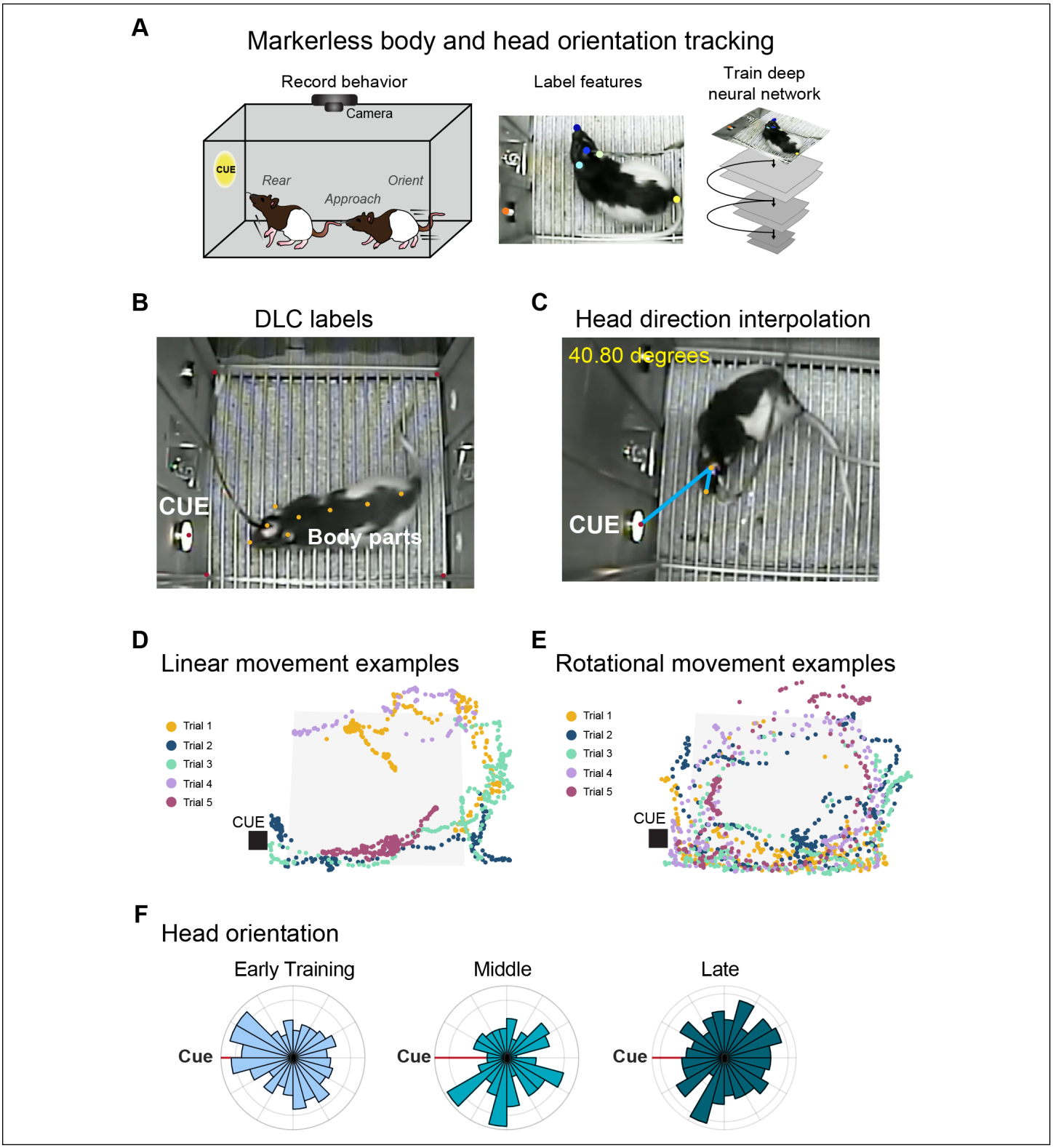

Supplementary Figure 2. Rat pose estimation and movement analysis. A) Behavior data was extracted from video recordings using the DeepLabCut pipeline. B) Video frames containing experimenter labeled rat body parts (ears, nose, tail base, etc) and static features of the environment (cue, chamber corners), were used to train a deep learning network to estimate frame by frame x,y coordinates for the entire video data set. This data was used to calculate movement and position information across optogenetic Pavlovian conditioning. C) Head direction was interpolated by calculating the angle between the vector projecting from the cranial implant to the nose with the vector projecting from the cranial implant to the cue. D) Example trials showing linear cue-evoked movement. Each dot represents the position of the rat's nose on an individual video frame, on 5 different trials early in training. E) Example trials showing rotational movement during 5 trials late in training. F) Polar plots showing distribution of head direction angles for an example rat across training.

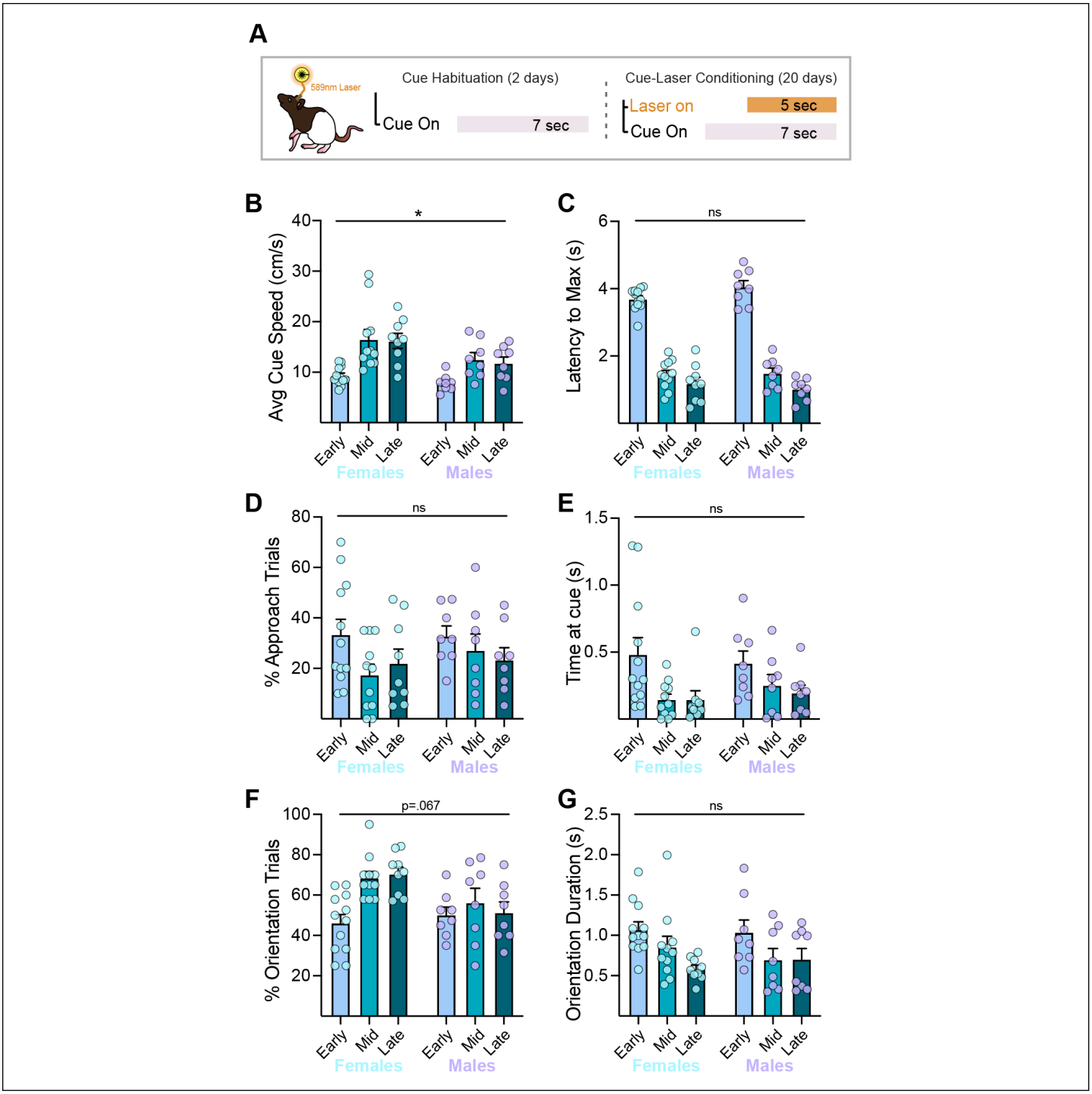

Supplementary Figure 3. Behavioral comparisons by sex. A) Behavior during optogenetic Pavlovian conditioning was analyzed as a function of rat sex. B) Females had higher average movement speed during cue presentations, compared to males, at all training phases. C-G) We found no other sex differences in behavioral measures, including the time to maximum movement speed, cue approach, or cue orientation.

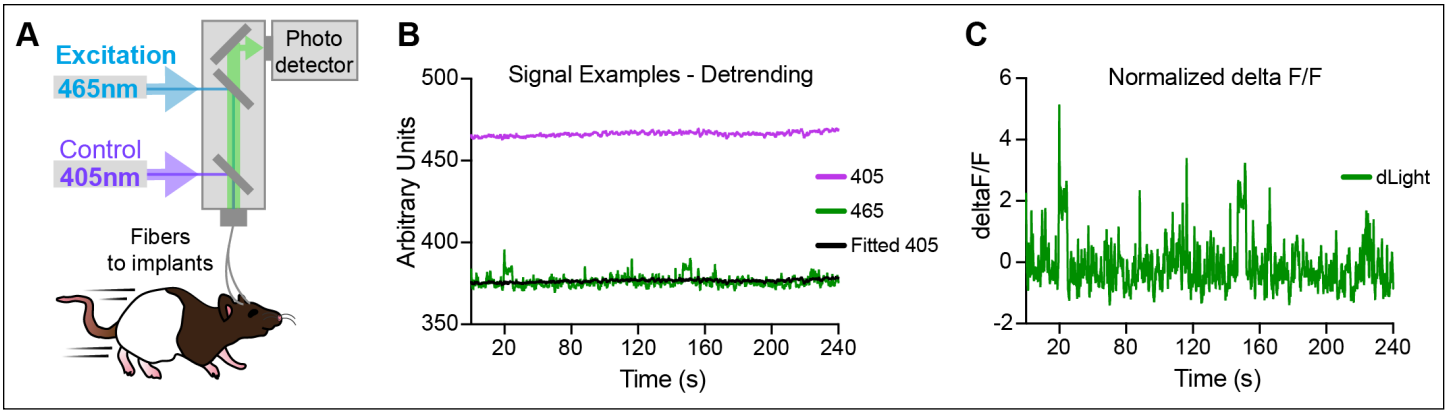

Supplementary Figure 4. Fiber photometry analysis. A) An AAV coding for expression of the dopamine biosensor dLight 1.3b was injected into striatal subregions, for in vivo measurement of dopamine-related GFP fluorescence during behavioral training. B) Example traces of raw demodulated 465-nm and 405-nm signals, and the 405-nm signal after applying a least squares fit (Fitted 405). C) Normalized 465-nm trace (deltaF/F) = (465 signal - fitted 405 signal)/(fitted 405 signal).

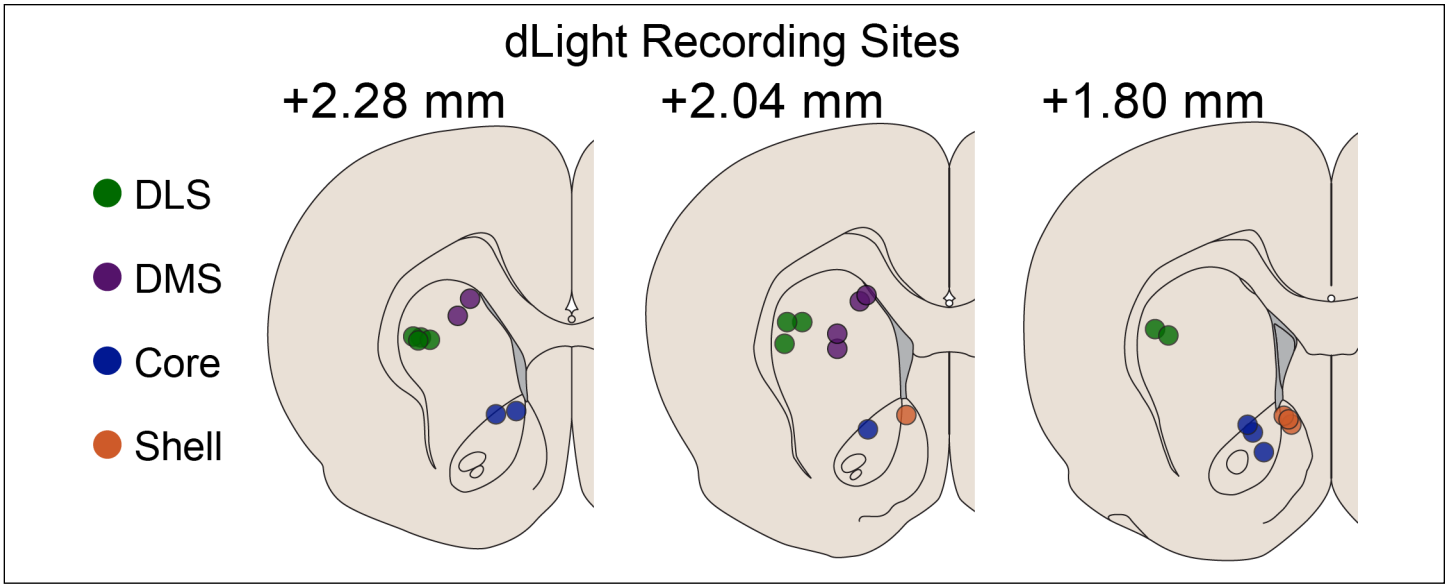

Supplementary Figure 5. Coronal atlas plates showing location of the tips of fiber optic implants for targeting dLight fiber photometry recordings to the nucleus accumbens core, nucleus accumbens medial shell, dorsomedial striatum, and dorsolateral striatum. Coordinates are in mm with respect to Bregma.

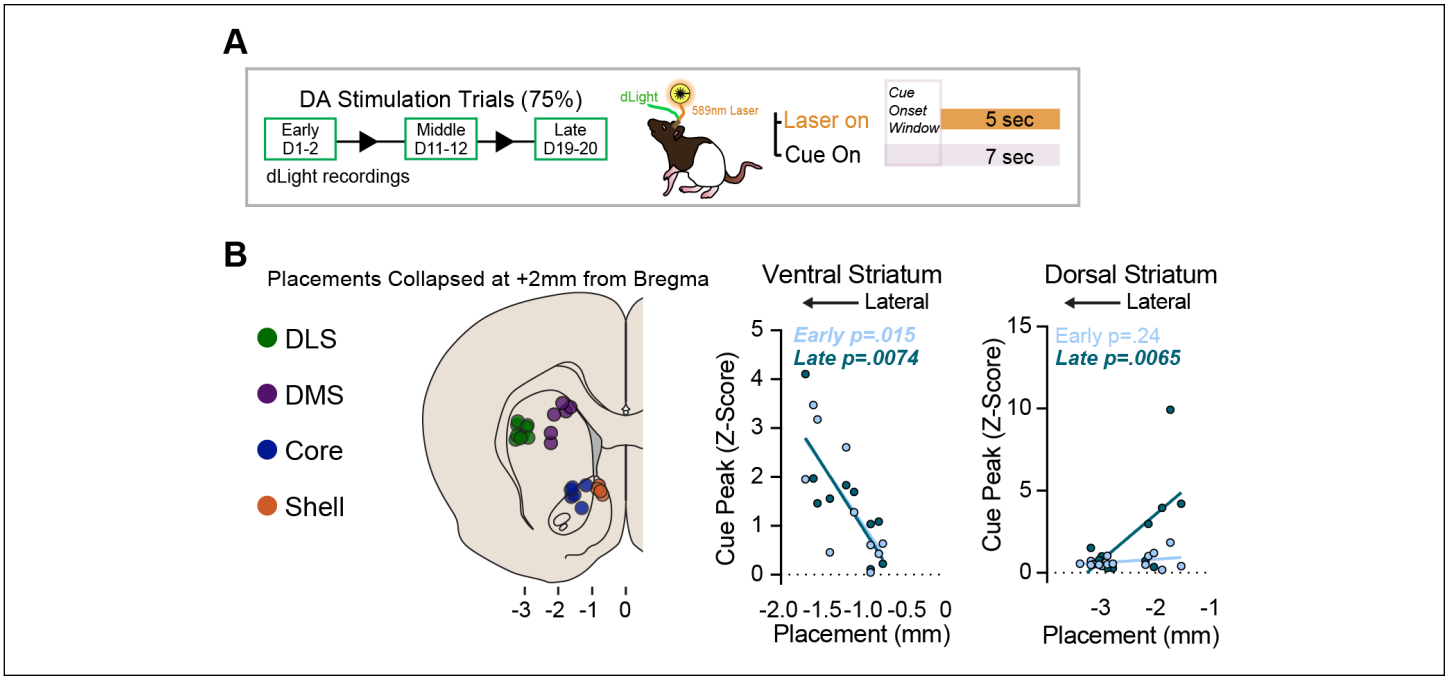

Supplementary Figure 6. Opposing gradients of cue-evoked dopamine signals in the ventral and dorsal striatum. Anatomical placements for all recording sites were collapsed onto a coronal atlas plate at +2.0mm from Bregma. The peak cue-evoked Z-scored dLight signal at each recording site was plotted against anatomical placement on the medial to lateral axis from Bregma. Opposing placement-signal relationships were found in the ventral and dorsal striatum after conditioning.

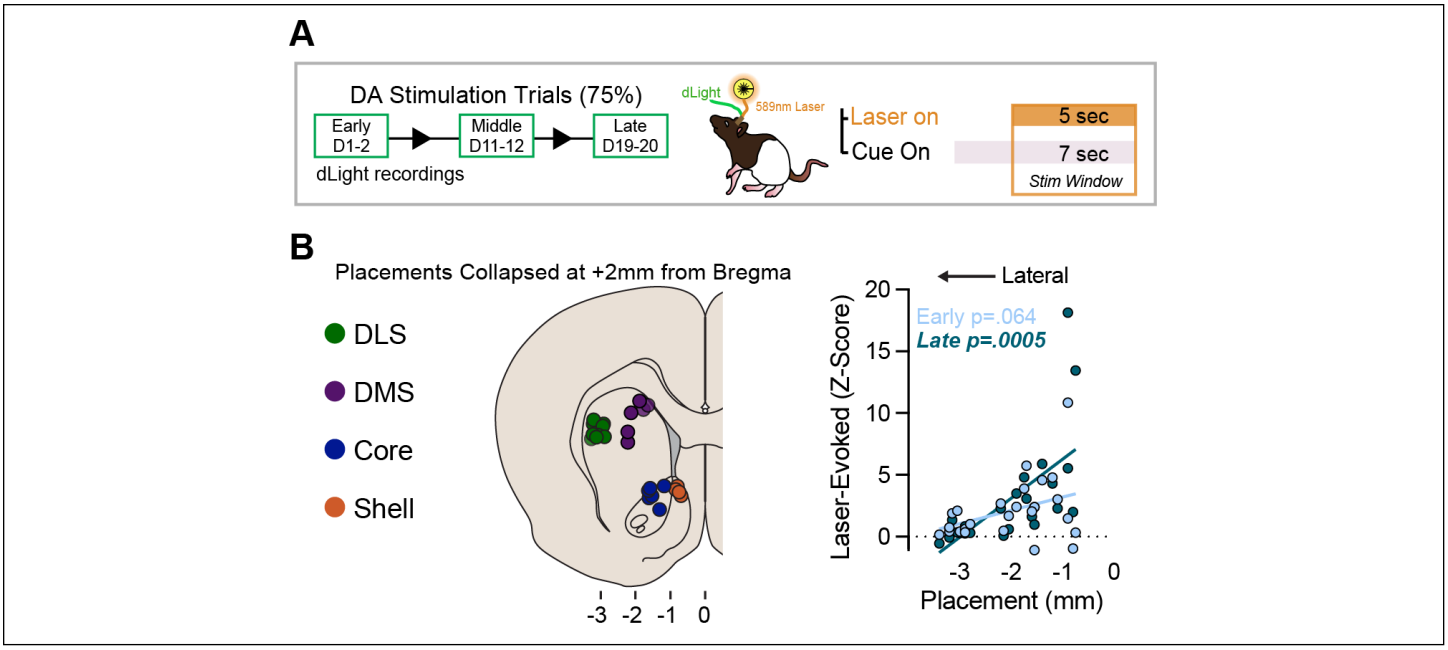

Supplementary Figure 7. A ventrolateral to dorsomedial striatal gradient of VTA dopamine neuron evoked dopamine signaling. Anatomical placements for all recording sites were collapsed onto a coronal atlas plate at +2.0mm from Bregma. The average Z-scored dLight signal during the laser stimulation periods at each recording site was plotted against anatomical placement on the medial to lateral axis from Bregma.